Modelling and Simulation of Ideal and Torque-limited Devices to Assist Elderly Walking

Tanaya Khanna

Thesis submitted to the University of Ottawa

in partial fulfilment of the requirements for the degree of

Master of Applied Science in Biomedical Engineering

Ottawa–Carleton Institute for Biomedical Engineering
Department of Mechanical Engineering
Faculty of Engineering
University of Ottawa

ABSTRACT

Interest in wearable exoskeletons is increasing as the demand increases for assistive technologies that meet the needs of the elderly population. Decreased mobility and loss of independence are major concerns as the global trend of increasing mean population continues. Past research has focused on walking assistance exoskeletons to maintain, restore, and enhance mobility. However, in the current state of the art, little is understood about how to best assist elderly individuals specifically. The results from studies of younger adults may not apply because gait patterns of elderly individuals often differ from those of the younger population. This thesis investigates the effect of ideal and torque-limited assistance on metabolic energy consumption when assistance is applied at the ankle, knee, and hip joints of elderly individuals during overground gait using the OpenSim software. The simulated ideal devices have no mass and can generate unlimited torque, representing a best-case scenario where the maximum amount of metabolic energy is saved given the observed kinematics. This simulation strategy provides an approximation of the upper limit for assistive devices that aim to reduce metabolic cost. The simulations with torque limits were generated to investigate the effect of this practical limitation. This study focuses on reducing metabolic cost as fatigue during walking is a fundamental concern in the elderly population. Simulations of 10 elderly participants walking at a self-selected, comfortable speed were generated using the Computed Muscle Control Tool in OpenSim. Ideal and torque-limited devices were added bilaterally at the ankle, knee, and hip joints of the 10 corresponding musculoskeletal models. The device torque profiles and changes in the activity and metabolic power consumed by the muscles were computed. The results of this study suggest that providing hip flexion/extension assistance to elderly individuals may result in substantially greater metabolic savings compared to assistance provided at the knee or ankle. When compared to the

unassisted simulations, the use of an ideal hip flexion/extension device resulted in a 24% average reduction in metabolic cost, with a loss in effectiveness of only 2 percentage points when the maximum torque was limited to 50% of the peak ideal torque; ideal hip abduction/adduction, knee flexion/extension, and ankle plantarflexion/dorsiflexion devices saved 15%, 20%, and 12%, respectively, on average. Computational studies of assistive devices can provide valuable insights for engineers who are developing walking assist exoskeletons for elderly individuals.

ACKNOWLEDGEMENTS

It gives me immense pleasure to express my deepest gratitude and sincere thanks to people who have always been supporting and encouraging me during my research work. This long journey of great opportunity would not have been possible without their support and encouragement.

This work would not have the spirit that it has without the invaluable academic support and belief in me as a graduate student, provided by my supervisors. I would like to express my sincerest gratitude to my supervisors, Dr. Thomas Uchida and Dr. Marc Doumit, for their support and guidance throughout my studies and investment in me throughout the process in helping me achieve my goals. Their expertise, constructive criticism and discipline proved invaluable to the progress of my work.

I would also like to extend my appreciation to the University of Ottawa and the Faculty of Engineering members for their contributions to my academic career. I thank my fellow graduate students and the members of my research team for their assistance and support throughout the program.

Most of all, I am indebted to my parents, brother, family, and friends for their patience, understanding, and unyielding support in helping me navigate these stressful times while I have worked towards reaching this milestone in my life.

DEDICATION

This thesis is dedicated to my supervisors, Dr. Thomas Uchida, Dr. Marc Doumit, and my parents, Dr. Pawan and Mrs. Poonam Khanna, who have inspired and motivated me to continue my path through higher education.

CONTENTS

LIST OF TABLES

LIST OF FIGURES

NOMENCLATURE

SYMBOL	DESCRIPTION
α	Pennation angle
Δm	Desired mass change
τ_a	Time constant that varies with activation level
τ_{act}	Muscle activation time constant
τ_{deact}	Muscle deactivation time constant
τ_j	Torque applied by the *j*th reserve actuator in CMC simulations
a	Muscle activation
a_i	Activation of the *i*th muscle
C_{calc}	Calculated metabolic cost
$\dot{E}_i(t)$	Rate of energy consumed by muscle *i*
f^M	Muscle force
$f^L(\tilde{\ell}^M)$	Active-force–length curve
$f^{PE}(\tilde{\ell}^M)$	Passive-force–length curve
$f^V(\tilde{v}^M)$	Force–velocity curve
F_{residual}	Force generated by residual actuator
J	Objective function
k_p	Feedback gain for position errors
k_v	Feedback gain for velocity errors
l_s^T	Tendon slack length
m	Mass
N_{mus}	Number of muscles
q	Vector of generalized coordinates
$\ddot{q}$	Coordinate accelerations
$\ddot{q}_{\text{exp}}$	Experimentally determined coordinate accelerations
q_j^{exp}	Experimental value for coordinate *j*
T	Duration of motion
u	Muscle excitation
w_i	Weight for marker *i*
w_j	Weight for coordinate *j*
x_i^{exp}	Experimental position of marker *i*
$x_i(q)$	Position of model marker *i*

ACRONYM	DESCRIPTION
BMI	Body mass index
C3D	Coordinate 3D file format
CMC	Computed Muscle Control
COM	Center of mass
DOF	Degree of freedom
GUI	Graphical user interface
IK	Inverse kinematics
MOT	3D motion file format
PE	Parallel element
RMS	Root mean square
ROM	Range of motion
RRA	Residual Reduction Algorithm
STO	OpenSim storage file
TRC	Track row column file
WAE	Walking assist exoskeleton

CHAPTER 1: INTRODUCTION

Chapter 1 discusses the changes in gait that have been observed in aging populations and the need for assistive devices that are designed specifically for elderly individuals. We describe the current state of the art in wearable assistive exoskeletons and current challenges. Finally, we describe the thesis objective, contributions and organization.

1.1. BACKGROUND

In Canada, elderly individuals represent a rapidly growing segment of the population. According to recent reports, elderly individuals are expected to comprise 23% to 25% of the population by 2036, and 24% to 28% by 2061 [1]. The average human age is rising globally, as are concerns about the decrease in mobility associated with aging. In particular, the need for medical resources may rise to unsustainable levels, which would have devastating impacts on society. The prevalence of gait and balance disorders increases with age, from around 10% between the ages of 60 and 69 years old to more than 60% in those over 80 years of age [1]. Gait impairments may greatly affect an individual's quality of life and may restrict personal independence [1]. Moreover, balance and gait impairments may lead to falling, which is the most common cause of severe injury in the elderly [2]. Walking is a sensitive indicator of overall health and an individual's self-selected, comfortable walking speed closely correlates with life expectancy in elderly individuals [3, 4]. One cause of frailty in elderly individuals is a reduction in daily physical activity such as walking, which in turn may be due to significant reductions in muscle mass and strength.

An individual's ability to remain active is a critical issue as it contributes to maintaining a good quality of life. Moreover, the increasing prevalence of obesity, arthritis, and diabetes combined with an aging population suggests that loss of mobility among elderly individuals has

become a serious social and economic issue whose importance may continue to increase. These concerns have led to growing urgency for assistive technologies to help elderly people perform activities of daily living and thus retain their independence. Various general-purpose exoskeletons that have been developed recently for applications like walking and running have been used to develop walking assist technologies for elderly individuals [5]. However, there is currently no commercially available exoskeleton that meets the requirements of elderly individuals and, thus, there is a need to develop assistive technologies for this population, which will ultimately reduce the burden on future healthcare services [5].

Recent advancements in sensing, actuation, and control technologies have enabled the development of wearable walking assist exoskeletons (WAEs) that improve gait performance and, ultimately, quality of life for the wearer. WAEs are mechatronic devices that apply forces to the body, thereby generating torques about the joints and reducing the amount of metabolic energy consumed by muscles during locomotion. The amount of metabolic energy consumed is referred to as "metabolic cost." WAEs may be categorized as being either powered or passive. Powered WAEs, often referred to as "exoskeletons," use portable batteries, sensors, actuators, and controllers to help the user walk; passive WAEs are constructed from similar components but have no net power contribution.

Several prototype devices, such as the Gait Enhancing Mechatronic System (GEMS) and the powered hip exoskeleton (PH-EXOS), apply assistive torques at the hip and have been developed specifically for elderly adults and individuals with gait disorders. However, most research has focused on young, healthy adults: the design considerations for assistive devices have not yet been standardized and characterized to meet the specific requirements of elderly walking assistance. To successfully translate existing technology to assist elderly individuals, WAE designs must be

informed by research that examines the effect of different assistive devices on elderly gait. Exoskeletons may require different assistance strategies to meet the needs of elderly individuals. Design approaches typically rely on experimental testing of physical prototypes; however, experiments may be limited in their ability to explain how design parameters affect device performance. Computational musculoskeletal modelling complements experiments by providing biomechanical explanations for observed effects [6]. Computational methods can provide insight into human–device interaction by determining the torques that should be generated by a device, estimating the energy expended by muscles, and predicting changes in muscle coordination.

1.2. OBJECTIVE

The purpose of this thesis is to study the effects of ideal and torque-limited actuation strategies applied at the ankle, knee, and hip joints in simulations of healthy elderly gait. The computational studies performed using the OpenSim software [7] will provide insight into the optimal assistive strategies for healthy elderly gait in order to improve future WAE designs.

1.3. CONTRIBUTIONS

The contributions of this thesis are as follows:

1. A thorough literature review was conducted to establish the current state of the art in walking assist devices for healthy elderly individuals and to investigate potential assistance strategies specific to the elderly population.
2. The OpenSim software was used to study the effects of adding an ideal actuator bilaterally (i.e., on both legs) at the ankle, knee, and hip to assist elderly gait. Metabolic cost was evaluated when unassisted and in various ideal assistance scenarios to predict the maximum metabolic savings that could be achieved by each type of device.

3. Ideal actuators were replaced with torque-limited actuators to predict the reduction in the metabolic benefit as the maximum motor torque decreases.

1.4. THESIS OUTLINE

This thesis contains five chapters. In this chapter, we have introduced our focus on elderly gait assistance strategies and have described the research objectives. Chapter 2 presents a review of the literature on elderly gait biomechanics, the current state of the art in WAEs and their application to the elderly population, and the use of computational methods that can complement experimental studies. Chapter 3 describes the OpenSim software, the musculoskeletal model used in this study, and the process for preparing motion data. This is followed by a description of the OpenSim computational workflow used in this study: Scaling, Inverse Kinematics, Residual Reduction Algorithm, and Computed Muscle Control. Chapter 4 presents and discusses the results obtained from the unassisted simulations and those using ideal and torque-limited devices. Chapter 5 concludes the thesis with a list of the contributions, the limitations of this study, and directions for future work.

CHAPTER 2: LITERATURE REVIEW

Chapter 2 presents a review of the literature on elderly gait. This chapter comprises four sections. The first section describes the walking gait cycle and gait phases. It is followed by a review of age-related changes in elderly gait and the kinematic and kinetic measurements that are used to quantify them. We then discuss the current state of WAE research and provide examples of powered and passive WAEs. Finally, the challenges of current WAEs and strategies that may be useful for assisting elderly individuals are discussed.

2.1. GAIT ANALYSIS

"Gait" refers to the characteristic cyclical walking or running patterns of a human or animal. It is important to assess and, where possible, treat individuals with conditions that affect their ability to walk since walking plays a crucial role in maintaining health and independence. Gait analysis describes the quantification and systematic study of key variables during gait. A walking gait cycle is defined by two consecutive foot contact events on the same leg, with foot contact of the opposite leg typically occurring halfway through. Each leg has a stance phase and a swing phase. The stance phase begins when the foot makes contact with the ground; the swing phase begins when the foot leaves the ground [8]. The walking gait cycle and its constituent events and phases are shown in Figure 2.1.

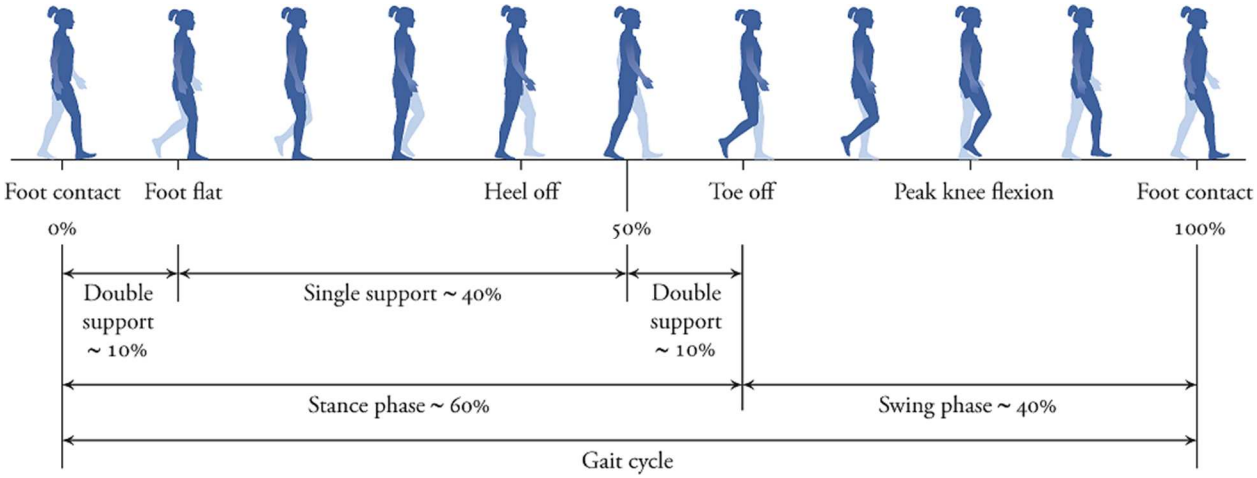

Figure 2.1. The walking gait cycle and its constituent events (e.g., foot contact) and phases (e.g., stance phase) [8]. Image © 2020 David Delp; used with permission.

The stance phase (from foot contact to toe off) comprises about 60% of the gait cycle in walking for a given leg. The swing phase accounts for the remaining 40% of the gait cycle. Because the stance phase is longer than the swing phase, there are periods in each walking gait cycle when both feet are in contact with the ground, known as double-support phases [8]. The intervals when only one foot is in contact with the ground are referred to as single-support phases. Important measures of gait include cadence (the rate at which foot contact events occur), walking base width (the lateral distance between the midpoint on each heel), step length (the distance along the line of progression between the same point on two consecutive footprints), stride length (the distance covered in one gait cycle) and walking speed (the product of stride length and stride frequency or, equivalently, the product of step length and cadence) [8, 9].

2.2. ELDERLY GAIT

Several age-related changes in one's physiology cause changes in gait. Studies have shown that age-related gait changes typically start occurring between the ages of 60 and 70 years old [10], often leading to loss of mobility in the elderly population. An important physiological change is a

loss of muscle strength, which may be attributed to a loss of motor neurons, muscle fibers, and/or aerobic capacity [2]. The structural weakening of lower-limb joints also affects mobility in elderly individuals. A lifetime of joint loading can result in degeneration of articular cartilage leading to diseases such as osteoarthritis, which reduce joint range of motion (ROM) [2]. Additional changes that are observed in elderly individuals are described in the sections that follow.

2.2.1. ELDERLY GAIT KINEMATICS

A kinematic analysis quantifies how the body segments and joints move during gait. Kinematic variables that often differ between elderly gait and the gait of young adults are listed in Table 2.1. On average, elderly gait is associated with slower speed, decreased step length and increased stance duration [11, 12]. The decline in walking speed as a consequence of normal aging is caused primarily by a decrease in step length rather than by a change in cadence [9]. In fact, cadence has been observed to remain relatively constant between young and elderly adults when walking at a self-selected moderate speed [9, 13]. JudgeRoy et al. [12] reported changes in the joint angles and ROM in the lower limbs of older adults (70–90 years old). JudgeRoy et al. reported a lower knee ROM in elderly adults (55 ± 5° compared to 59 ± 5° in young adults) and a lower peak plantarflexion angle in elderly adults (13 ± 5° compared to 17 ± 5° in young adults) [12]. Prince et al. [2] noted that ankle ROM is lower in elderly adults than in younger adults (24.9° vs. 29.3°) and hip ROM is higher (40° vs. 32°). An increase in hip ROM with aging can be attributed to an increase in anterior pelvic drop, resulting in increased hip extension [2].

Variable	Value		Age Group ANOVA (p-value)	Age Group Effect (95% CI)
	Young Adults (N=32)	Elderly Adults (N=26)		
Age (years)	26 ± 6	79 ± 6		
Body mass (kg)	64.9 ± 11.6	65.7 ± 11.7	0.79	
Height (cm)	166 ± 10	158 ± 9	0.005	3.4 (1.2, 6.5)
Gait speed (m/s)	1.16 ± 0.13	1.03 ± 0.13	<0.001	0.09 (0.03, 0.14)
Step length (proportion of leg length)	0.74 ± 0.04	0.65 ± 0.07	<0.001	0.06 (0.04, 0.08)
Single-support time (percentage of gait cycle)	40 ± 2%	37 ± 3%	<0.001	2.0 (1.1, 3.0)
Hip range of motion	42 ± 3°	43 ± 5°	0.58	
Knee range of motion	59 ± 5°	55 ± 5°	<0.001	2.9° (1.3°, 4.5°)
Peak ankle plantarflexion angle	17 ± 5°	13 ± 5°	0.002	2.9° (1.1°, 4.7°)

Table 2.1. Kinematic variables reported in young and elderly adults during comfortable-speed walking (mean ± standard deviation; other statistics stated where provided) [12].

2.2.2. ELDERLY GAIT KINETICS

Kinetic variables of gait describe the internal and external forces that are responsible for producing observed joint motions [10]. Experimental studies have reported that the effect of aging on the hip results in an increase in hip flexion power and moment during the late stance phase of walking (as compared to young adults) [12]. Table 2.2 compares the kinetics reported by Prince et al. [2] for 18 healthy elderly participants when walking with their natural cadence to the same variables observed in 9 young adults. On average, the peak ankle plantarflexion moment decreased from 1.63 N·m/kg in young adults to 1.44 N·m/kg in elderly individuals and resulted in a “significantly

less vigorous push-off" [2]. Winter et al. [14] reported a lower plantarflexion power of 2.478 W/kg during elderly walking, compared to 3.266 W/kg in young adults. Judge et al. [12] reported a similar reduction as Winter et al. in plantarflexion power during walking at a comfortable pace: 2.9 ± 0.9 W/kg in elderly individuals (N=26, average age 79) compared to 3.5 ± 0.9 W/kg in young adults (N=32, average age 32). Prince et al. [2] also noted that the work done by ankle plantarflexor muscles is lower in elderly individuals (0.190 J/kg compared to 0.293 J/kg in young adults) [2]. A 20–40% reduction in skeletal muscle strength has been observed in older adults at age 70 [15]. Thus, the reduction in ankle power observed in elderly gait during push-off may be due to a reduction in skeletal muscle strength [12].

Variable	**Value**	
	Young Adults (N=9)	**Elderly Adults (N=18)**
Mean age (years)	22	71
Peak plantarflexion moment (N·m/kg)	1.628	1.437
Peak plantarflexion power (W/kg)	3.266	2.478
Plantarflexion work (J/kg)	0.293	0.190

Table 2.2. Kinetic variables reported in young and elderly adults during comfortable-speed walking (mean) [2]. Moment, power and work are normalized by subject mass.

2.3. ASSISTIVE DEVICES

The need for developing wearable assistive devices is increasing due to the global trend of a growing elderly population. The biomechanical changes due to aging result in decreased mobility, which can make daily activities such as walking extremely difficult. Assistive technologies have the potential to help elderly people retain their independence by improving mobility. Assistive

devices can compensate for muscle weakness by reducing the load on the lower extremities or by applying moments to the biological joints. Assistive devices aim to reduce disability, decrease the burden of care, and enhance mobility, balance and stability. Improvement in cardiorespiratory functions (with enhanced circulation of blood/fluids) along with psychological benefits have also been reported by patients using these devices [16]. An improved confidence level and feelings of safety, resulting in increased daily activity and independence, have also been reported [16].

Assistive devices are used by a wide range of patient groups, including individuals with spinal cord injuries, stroke, and osteoarthritis. Although assistive technology holds promise for older adults, it is important to understand how well existing and proposed devices will meet their needs. It is critical to develop assistive devices to help healthy individuals avoid gait deterioration associated with aging. WAEs can be classified as either powered or passive devices; examples of existing powered and passive WAEs are discussed below.

2.3.1. POWERED WAEs

Powered WAEs are portable devices comprised of batteries, sensors, actuators, and controllers mounted to rigid and flexible mechanical systems that help the wearer to walk or run. The Gait Enhancing Mechatronic System (GEMS) developed by Samsung is a typical example, functioning as a wearable hip assist robot [17]. The GEMS device consists of two actuators that generate assistive power at the left and right hip joints, a brace that fits around the waist, a pair of thigh frames that transmit assistance torque from the actuators to the thighs, and fabric belts at the ends of the thigh frames (see Figure 2.2). The electronic components such as the battery and controller hardware are worn on the back. The total system mass is 2.8 kg. Two 70 W motors are mounted near the hip joints to generate the assistance torque, which is transmitted through a multi-stage gear system. Each joint has one active degree of freedom (DOF) for hip flexion/extension (i.e.

rotation in the sagittal plane) and one passive DOF that permits hip abduction/adduction (i.e. rotation in the frontal plane; see Figures 2.3 and 2.4 (A)) [17]. Although the GEMS device provides assistance at only the hip joint, it was found to reduce activity in muscles crossing the knee and ankle in addition to the hip flexors and extensors [17].

Figure 2.2. The Gait Enhancing Mechatronic System (GEMS) hip assist robot [17]. Copyright © 2017, IEEE; used with permission.

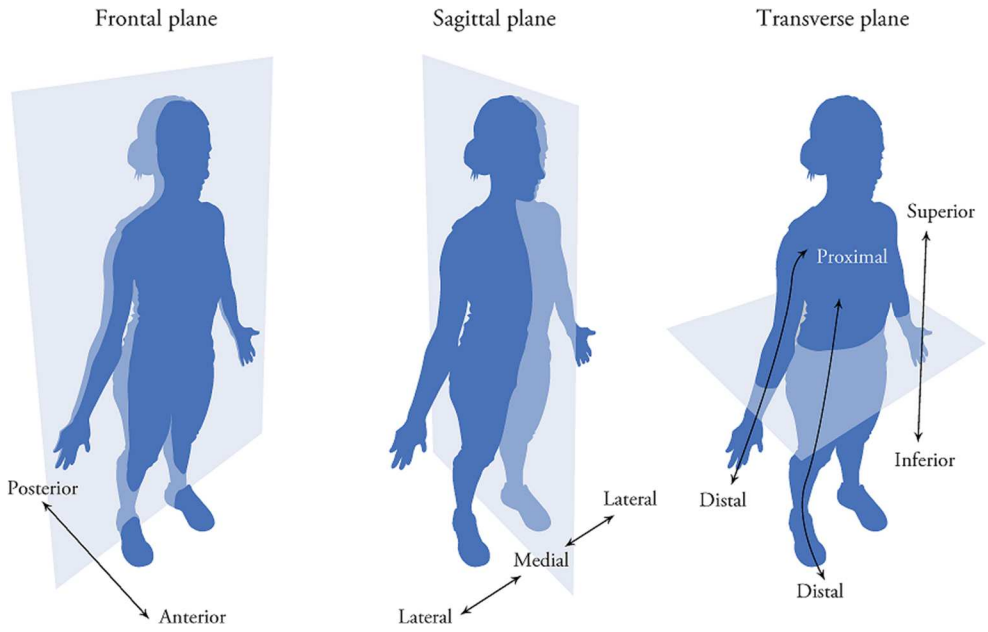

Figure 2.3. Anatomical planes and directions in a human [8]. Image © 2020 David Delp; used with permission.

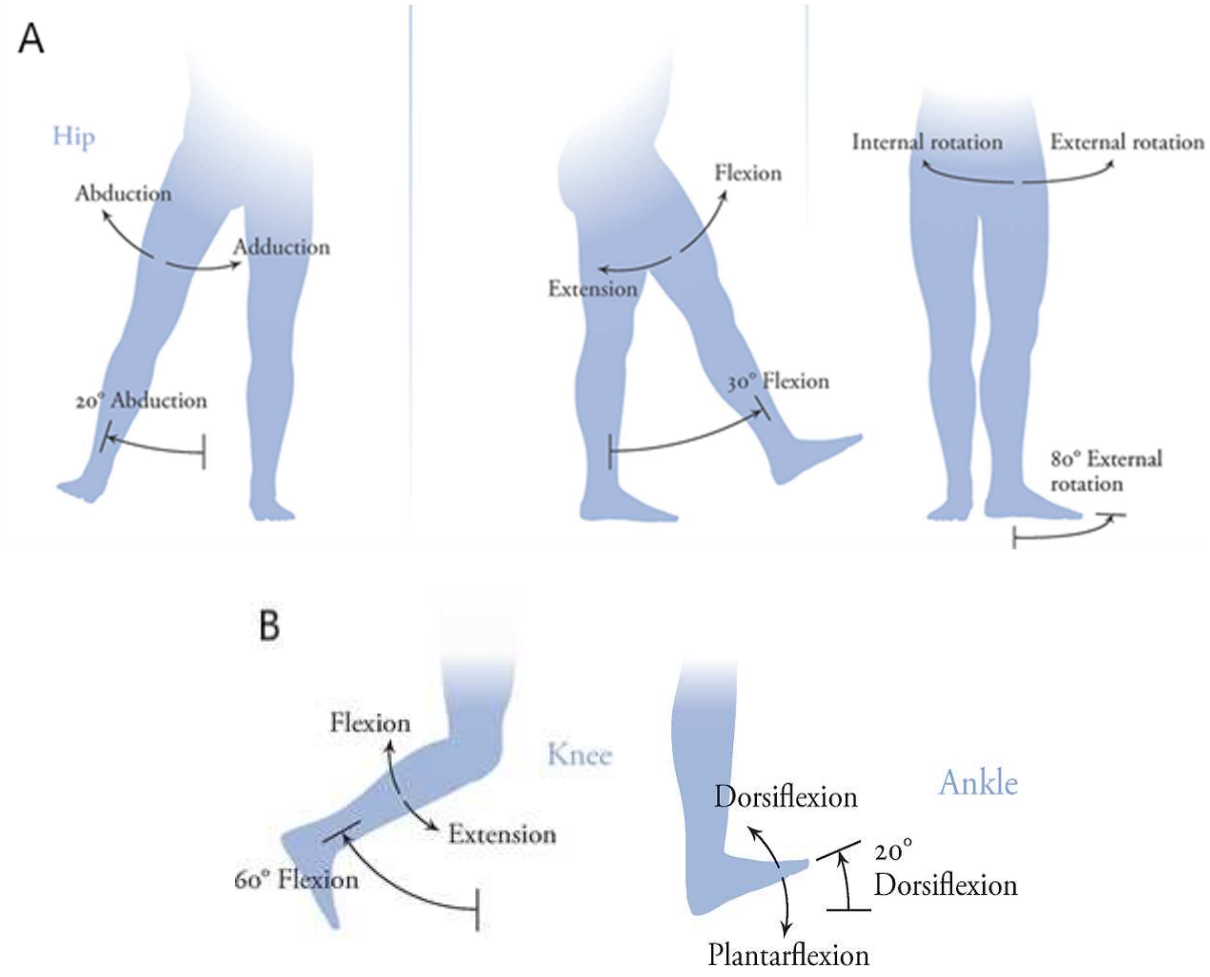

Figure 2.4. Motions of the hip in the frontal plane (left column), sagittal plane (center column), and transverse plane (right column) (A). Motion of the knee (left) and ankle (right) in the sagittal plane (B) [8]. Image © 2020 David Delp; used with permission.

Wu et al. [18] proposed a powered hip exoskeleton (PH-EXOS) with the objective of assisting the lower-limb motion of individuals with walking impediments. The mechanical structure of PH-EXOS is designed to be anthropomorphic to provide natural-feeling walking assistance for the user [18]. Servo motors and flexible Bowden cable transmission systems were used to ensure the system has low inertia, a compact structure, and high-performance actuation. As shown in Figure 2.5, the device comprises two passive DOFs at each hip joint (internal/external rotation and abduction/adduction) and one active DOF (flexion/extension). A universal joint is used at each hip

to permit motion of the two passive DOFs [18]. The motors are mounted behind the backpack frame, which has high structural rigidity to support the applied torques. The motors are controlled based on the signals from sensors that measure the human–robot interaction forces and predict the intended motion of the user.

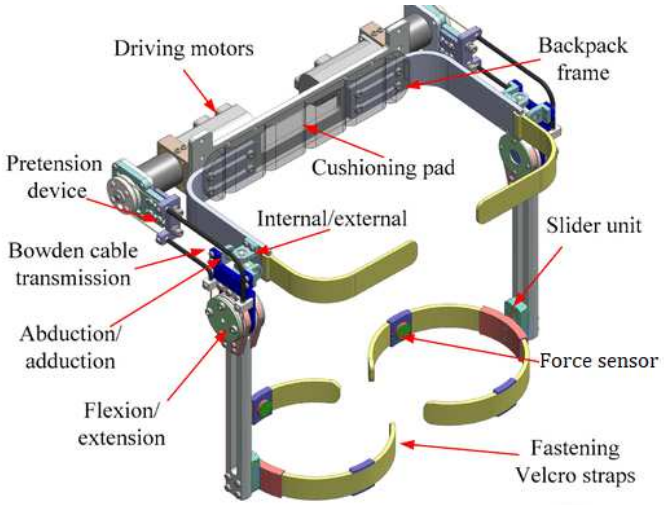

Figure 2.5. The architecture and major components of the PH-EXOS powered hip exoskeleton [18]. Image © 2015 Q. Wu et al.; used with permission.

The walking assist device developed by Honda was designed to improve walking efficiency (Figure 2.6). The device was designed based on an inverted-pendulum model of walking. During bipedal gait, the stance limb is represented by an inverted pendulum that is pinned to the ground at the ankle, allowing the limb to rotate about the ankle in the sagittal plane; the stance-limb knee is often assumed to remain locked in a fully extended position. The swing limb is modelled as a double pendulum, with the thigh and shank segments pin-connected at the knee [8]. The body exchanges potential energy for kinetic energy and minimizes the role of muscles during the swing phase in order to achieve smooth and efficient bipedal walking [8, 19]. Honda's device weighs approximately 2.7 kg and consists of adjustable frames, making it possible for people with various body sizes to use the device. The wearer's gait is controlled by a central pattern generator (neural

networks that generate rhythmic patterns of output, independent of sensory feedback) and two electric motors, which generate simultaneous and complementary torques that are applied at the hips of the user via thigh frames. A computer controls the activation of the motors based on data obtained from sensors on the legs, providing hip flexion/extension assistance and improving gait symmetry. Hip joint angle and electric current sensors monitor the range of motion of the user's hip joints and the motor torques, respectively, throughout the gait cycle to regulate the walking motion [19, 20]. Significant improvements have been reported in several spatiotemporal gait parameters, including velocity, cadence, step time, stance time, swing time, double-support time, stride length, and spatial asymmetry, when tested on healthy individuals between 18 and 85 years of age when walking at speeds of 0.4–0.8 m/s [20].

Figure 2.6. Honda's walking assist device [20]. Copyright© 2015, Buesing et al.; used with permission.

2.3.2. PASSIVE WAEs

Passive WAEs are devices that complement the wearer's gait using passive mechanical components such as springs, clutches, levers, and pulleys. Passive exoskeletons assist the user by storing and subsequently returning mechanical energy to the user without injecting net positive mechanical work [21]. Some passive devices use elastic components that store and release energy as the person walks. In contrast to powered WAEs, which are limited by their battery operating time and are often bulky and complex, passive WAEs are generally simpler, less expensive and lighter. Examples of passive WAEs are the XPED2, the MoonWalker and the passive ankle exoskeleton from Collins et al. [26], which are described below.

The assistive strategy of the XPED2 exoskeleton is to reduce the muscle-generated joint torques using elastic elements called exotendons [22], which are long, elastic cables that replicate the mechanical behaviour of multi-articular muscle–tendon units. The cables can effectively store and transfer power across multiple joints. The XPED2 was developed to test the prediction that a triarticular exotendon (crossing the hip, knee, and ankle) can reduce joint moments by 46% [23]. The exotendon extends from a lever at the pelvis to a leaf spring at the ankle, via a pulley at the knee (see Figure 2.7). The cable is loosened during hip flexion and ankle plantarflexion and is tightened during hip extension and ankle dorsiflexion (Figure 2.4(B)). During the transitions between heel strike and midstance, the exotendon stretches and stores energy; this energy is then released during the terminal stance phase [23]. The total mass of this device is 6.91 kg. A reduction of 12.1% in average absolute joint torque was measured when tested on six young participants with an average age of 21. The large difference between the theoretically predicted savings (46%) and the savings observed experimentally (12.1%) is typical.

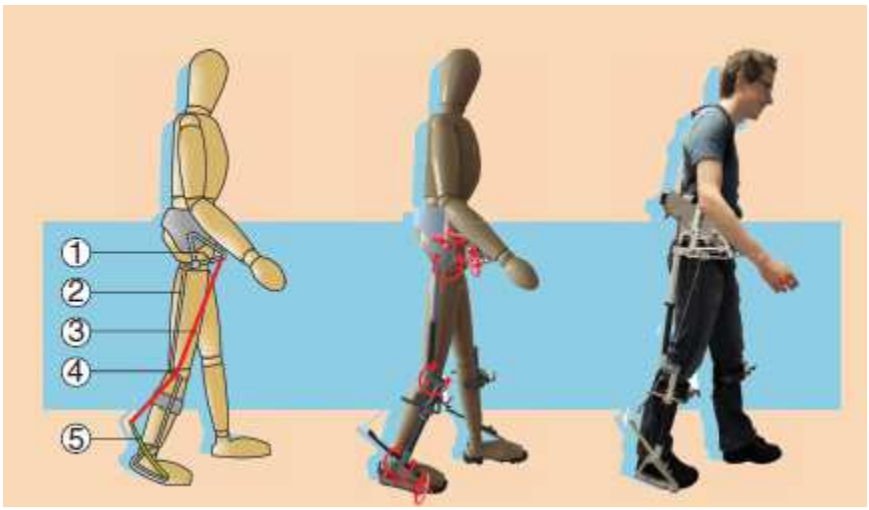

Figure 2.7. The XPED2 exoskeleton: schematic (left), computer-aided design model (center) and photograph of a participant wearing the device (right). Numbers in the left panel indicate (1) pelvis lever, (2) rigid frame, (3) exotendon, (4) knee pulley, and (5) foot leaf spring [23].

The MoonWalker is a "quasi-passive" WAE proposed by Krut et al. [24] that provides assistance by supporting a portion of the wearer's body weight. The design philosophy of the MoonWalker was to convert a conventional body-weight support system used in gait rehabilitation into a mobile structure. The device consists of four subsystems: two leg structures, two custom shoes, a force balancer and a force-sharing mechanism (Figure 2.8). The two leg structures are curved so as to avoid interfering with the motion of the wearer's legs during gait. Spherical (ball-and-socket) joints connect the "rigid shoes" to the "curved sticks" (labelled in Figure 2.8) to allow the ankle to move naturally [24, 25]. A "force balancer" is mounted to a rigid plate and attached to a harness worn by the user. The force balancer consists of a spring and prismatic joint that are tuned to help support the body's weight. An initial prototype provided an upward force of 320 N during midstance [24, 25]; however, the system was very noisy, the harness unit caused discomfort and the resulting gait pattern was unstable.

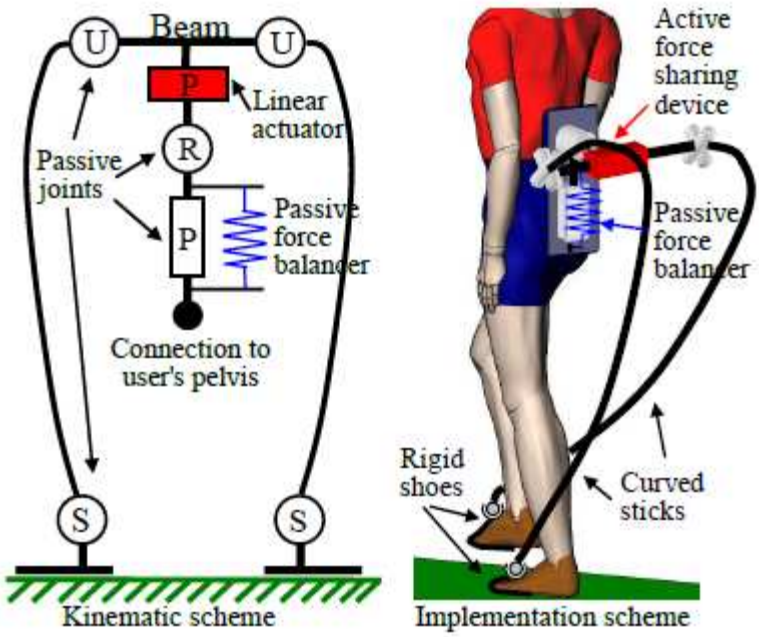

Figure 2.8. Schematics of the MoonWalker [24]. S, U, P and R indicate spherical, universal, prismatic and revolute joints, respectively. Copyright © 2010, IEEE; used with permission.

Collins et al. [26] designed a lightweight passive ankle exoskeleton that provides some of the functions of the calf muscles and tendons during walking. The device aims to reduce the high energetic demands of the calf muscles during push-off using only 4 passive components: a carbon fiber frame, an extension spring, a rigid cable and a mechanical clutch (Figure 2.9). The upper portion of the frame wraps over the top portion of the calf muscles of the user. The lower portion of the frame is in the shape of a foot orthosis and is placed inside the wearer's shoe. The upper and lower portions of the frame are connected by a 1-DOF joint that allows only plantarflexion and dorsiflexion of the ankle [26]. As the shank rotates during mid- and terminal stance, the clutch is engaged and the spring stretches to store potential energy. During pre-swing, this energy is released, and the clutch is disengaged. This assistance strategy was inspired by ultrasound imaging studies that suggest the muscle fascicles behave like clutches to hold the spring-like Achilles tendon, the recoil of which leads to the largest burst of positive mechanical power at any joint during walking [27]. The device was tested on healthy participants walking on a treadmill. The

two prototypes used during testing had masses of 0.408 kg and 0.508 kg, and reduced metabolic energy expenditure by 7.2% (average over 9 participants) when using a spring stiffness of 180 N/m [25, 26].

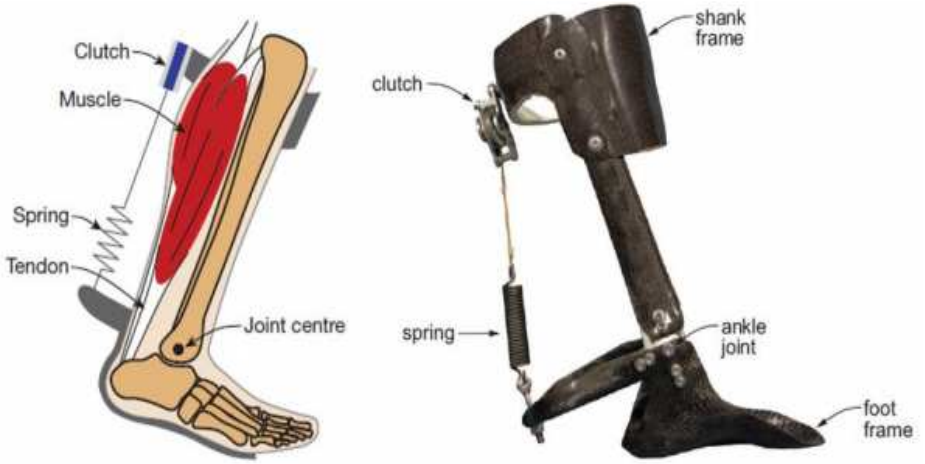

Figure 2.9. Schematic of the passive ankle exoskeleton (left) and photograph of one of the prototypes used during walking trials (right) [26]. Copyright © 2015, Nature Publishing Group, a division of Macmillan Publishers Limited. All Rights Reserved; used with permission.

The devices described above are a few prominent examples of the recent advancements in wearable assistive devices. The development of assistive technology is an emerging field of research, driven by an aging society and an increase in the number of patients with impaired mobility. However, the design process has not yet been standardized. WAEs assist different joints of the lower body and have different design philosophies. Specific age-related changes that are observed in the lower extremities of elderly individuals must be considered to develop effective assistive strategies for this population.

2.3.3. CURRENT STATE OF WAEs

One of the aims of assistive device designers is to reduce the metabolic cost of walking. However, this aim is difficult to achieve, as a robotic device must be carefully designed to interact

harmoniously with finely tuned biological systems—a feat that has been accomplished only relatively recently [6]. Device designers are making progress on overcoming the issue of subject-to-subject variability in performance, but understanding the musculoskeletal adaptations that occur when the body is augmented with an assistive device remains a major challenge [6]. For example, even if a device reduces muscle activity, it may not reduce metabolic cost or muscle fiber power [6]. Researchers have used experiments to learn a great deal about providing assistance during gait. For example, it is known that device effectiveness can be sensitive to actuation timing, metabolic cost can be reduced with a passive device [26], and unilateral assistance (i.e., applied to one leg only) can affect the activity of muscles on the unassisted leg [6].

Experimentalists have suggested strategies to assist elderly walking based on the changes in gait associated with aging. One strategy is to provide assistance at the ankle in healthy elderly individuals, which may increase walking speed and compensate for the reduced strength of the plantarflexor muscles [12]. Other studies have suggested that assisting the hip joint may improve gait symmetry in elderly adults with movement impairments, and assisting at the hip of elderly individuals with osteoarthritis may reduce the stress on the hip joint [11]. However, it is challenging to determine optimal assistance strategies using experiments alone, as designing and prototyping devices is expensive and time-consuming [26]. Moreover, human testing introduces additional obstacles, such as obtaining ethics approval, recruiting participants, guaranteeing subject safety, and building subject-specific prototypes [26].

Simulation-guided design can overcome the above challenges by reducing the need to build physical prototypes and enabling fast, automated, and repeatable testing without risk of injury. Simulations have revealed the distribution of energy consumption during walking between stance and swing phases [6], and we can explore hypothetical ideal devices that are massless, provide

lossless transmission of torque to the limb, and have no torque or power limits. Thus, the effectiveness of different devices (e.g., hip vs. knee assistance) over many subjects can be compared, and independently from the many practical challenges that face experimental studies [28, 29].

In this study, OpenSim simulation tools have been used to explore possible assistance strategies for healthy elderly gait. The musculoskeletal simulations were used to overcome experimental challenges and provide insight into the design criteria of WAEs for elderly individuals. An ideal assistance strategy should reduce the metabolic energy expended by the muscles, thus reducing the effort required by the wearer. The design and development of WAEs for elderly individuals will lead to enhanced mobility to perform activities of daily living and improvement in the overall quality of life.

2.4. SIMULATIONS OF GAIT

Several prototype iterations are typically required to develop an exoskeleton and it is challenging to determine how to improve the design parameters [5]. The performance of current WAEs are limited by both technical and conceptual challenges. For example, a common technical challenge is reducing the mass of the device, which can limit the device's ability to reduce metabolic cost. Another concern is generating torques whose timing and magnitude complement the moments generated by the muscles. The problem is particularly challenging for WAEs as the system must be lightweight and portable. Passive WAE designers have also encountered issues synchronizing the assistive torques with the gait cycle [25]. It is difficult to create a reliable timing mechanism that ensures optimal energy release because gait varies among individuals.

An inverse dynamic analysis is often used to understand how best to assist muscles during gait. However, such an analysis computes only net joint moments and powers: it does not explain

which muscles are acting and with what amounts of force [30]. An inverse dynamic analysis must be combined with models that include the effects of biological tissues in order to better quantify walking. Few models are available to quantify and evaluate the interactions between an exoskeleton and the limbs of the user. For this reason, experimental gait data are still necessary to study the human–device interaction. However, human experiments are expensive and time consuming. Moreover, data from experimental trials alone may limit our ability to understand movement dynamics because many important variables (e.g., the forces generated by each muscle) are not generally measurable. Finally, it is difficult to establish cause–effect relationships in complex dynamic systems from experimental data alone [31]. These challenges can be addressed by a computational analysis of the musculoskeletal system, which can then allow one to determine valuable information about exoskeleton design requirements.

Computational musculoskeletal modelling is an important tool, complementing experimental research by providing parametric and predictive models that can accelerate the design process. A few simulation and modelling software packages are in common use, notably Visual 3D (C-Motion, Inc.), BoB (Biomechanics of Bodies), AnyBody (AnyBody Technology) and OpenSim (Stanford University). Visual 3D is a dynamic simulation software application that is often used to analyze 3D motion capture data. It is designed to manage data from marker set systems to facilitate calculation of joint angles and moments using inverse dynamics but is unable to compute muscle forces. Visual 3D musculoskeletal models are comprised of body segments that float in space and can apply forces to other segments [32].

Biomechanics of Bodies (BoB) has the simplest interface of the tools listed above. It allows users to calculate movement trajectories, joint torques, muscle activations, and joint contact forces.

BoB is written in MATLAB, which enables data to be easily exported and analyzed using MATLAB's built-in capabilities [33, 34].

AnyBody is a sophisticated skeletal modelling software package but requires a paid license. It analyzes musculoskeletal systems as rigid-body systems and can calculate many quantities of interest. In addition to performing inverse kinematics and inverse dynamics calculations, it is also capable of estimating muscle forces. The anatomical properties of the default human model, such as its height, weight, segment lengths, strength, and bone geometries, can be adapted to suit the needs of the user. Another feature of this program is its ability to model the simulation environment. STL files that define 3D geometries can be imported into the program to simulate objects or assistive devices that may affect the model [33].

OpenSim is an open-source simulation software package that allows users to build, modify, and share musculoskeletal models. Researchers have developed and validated several generic models that are released with OpenSim, including models of the upper extremity [35], lower extremity [36], and full body [37]. Additional models, contributed by members of the biomechanical modelling community, are available for download on the OpenSim website. Like AnyBody, OpenSim can compute inverse kinematics, inverse dynamics, and muscle forces. The program can also perform optimizations and generate predictive forward dynamic simulations [31]. The OpenSim framework was adapted from SIMM, an older simulation platform that was used to build, analyze and modify musculoskeletal models. However, it was not able to compute muscle excitations and its source code was not exposed to users, making it difficult to extend and improve the platform [33]. OpenSim was selected for this research since it is an open-source platform with low-level computational tools that are easily accessible through a graphical user interface [31].

CHAPTER 3: METHODS

This chapter describes the methodology used to generate the simulations in OpenSim. An overview of OpenSim and its musculoskeletal models is provided, then the typical process by which motion capture data are collected and used to generate a simulation is described. The simulation workflow comprises four main OpenSim Tools: Scaling, Inverse Kinematics (IK), Residual Reduction Algorithm (RRA) and Computed Muscle Control (CMC). Finally, modelling of two types of assistive devices is described: ideal devices and devices with torque limits.

3.1. OPENSIM

OpenSim is an open-source, freely available musculoskeletal modelling and simulation software package that allows one to build, analyze and modify models of a wide range of musculoskeletal structures [31, 38]. It allows one to calculate and analyze joint motions from motion capture data and estimate variables that cannot be measured directly such as muscle activations and joint loads. Such variables are difficult to study using experimental data alone. In this work, the OpenSim software was used to generate muscle-driven simulations from motion data of healthy elderly walking, then to investigate the energy consumed by muscles during unassisted gait, when assisted by ideal actuators, and when assisted by torque-limited actuators. The OpenSim Tools were used to generate and validate the muscle-driven simulations, and to obtain insight about assistance strategies for elderly gait.

3.2. OPENSIM MODELS

An OpenSim model consists of components that correspond to parts of a physical system, such as rigid bodies, joints, forces, contact surfaces, markers, and controllers (Figure 3.1) [38, 39].

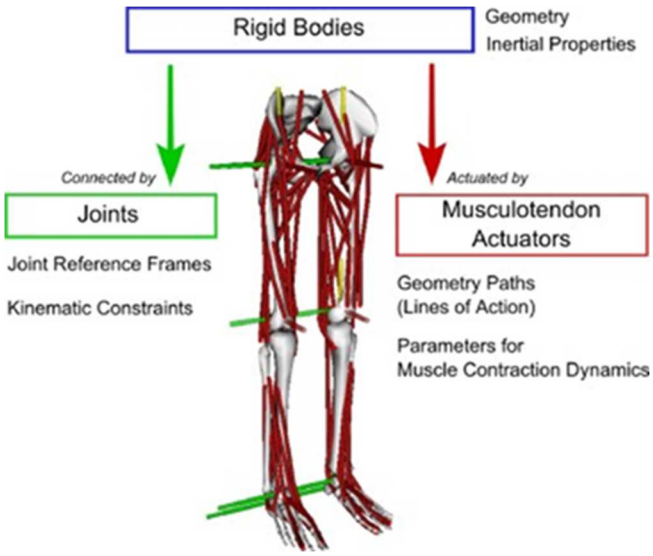

Figure 3.1. Components of a typical OpenSim model [39]. © 2017 Elsevier B.V. All rights reserved; used with permission.

The "Gait2392" musculoskeletal model was used for this study because we focus on analyzing the lower limbs during elderly gait. This model has been used successfully in similar studies [29, 40] and has been carefully validated in the literature [41]. Figure 3.2 shows the generic Gait2392 model, which represents an individual with a height of 1.8 m and a mass of 75.16 kg. The Gait2392 model has 23 degrees of freedom and includes 92 musculotendon actuators that represent 76 muscles in the lower extremities and torso [36]. The knee has only 1 DOF but it translates along and rotates about the other axes as it flexes and extends to replicate the motion of the articulating surfaces of the femur and tibial plateau (see Figure 3.3) [8].

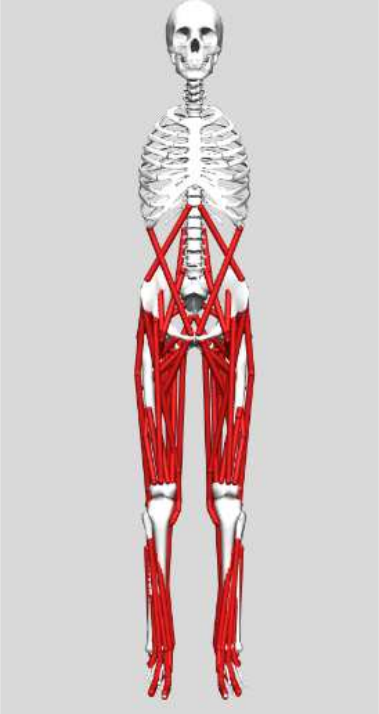

Figure 3.2. The Gait2392 musculoskeletal model in its default pose in the OpenSim GUI.

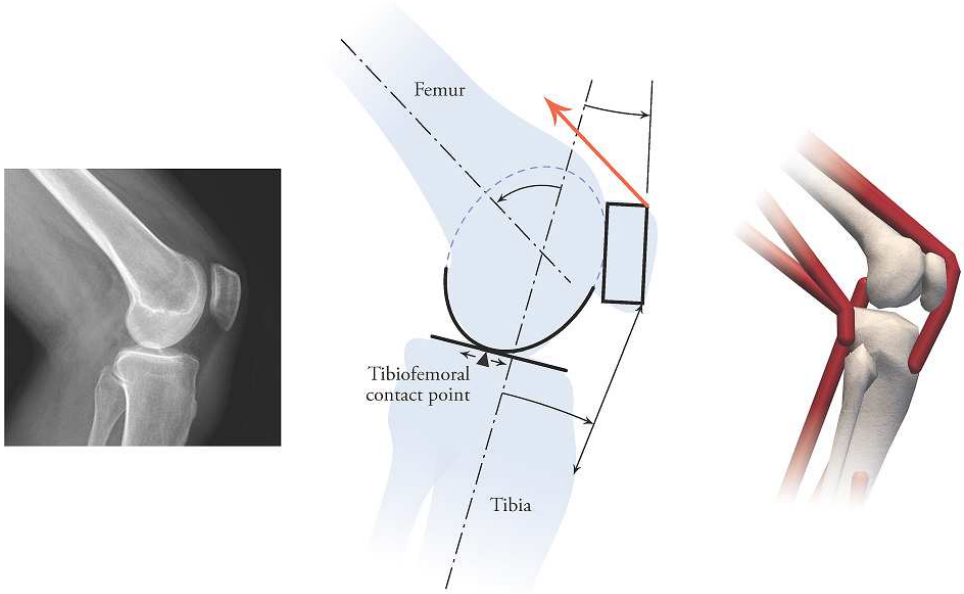

Figure 3.3. The complex biological contact surfaces in the knee (left), a mathematical description of the geometry (center) and a musculoskeletal model based on the mathematical description (right) [8]. Image © 2020 David Delp; used with permission.

The Full Body Model by Rajagopal et al. [37] is another candidate for studies of gait. This model has 37 degrees of freedom, 80 musculotendon actuators actuating the lower body, and 17 ideal torque actuators driving the upper body [37]. The Full Body Model was developed only recently and, as such, relatively few validation studies have been performed. The Gait2392 model has been used extensively and thus there exists a corpus of literature from many experimental studies with which one can compare new simulation results.

3.2.1. ACTIVATION DYNAMICS

The Gait2392 model uses a simplified first-order activation dynamic model. An idealized muscle excitation signal (u), a dimensionless quantity between 0 and 1, is used as the input to each of the muscles. The muscle excitation is related to the muscle activation (a), which also lies between 0 and 1 and is expressed by a nonlinear first-order differential equation [48]:

$$\frac{da}{dt} = \frac{u - a}{\tau_a(a,u)} \tag{3.1}$$

where $\tau_a(a,u)$ is a time constant that varies with activation level:

$$\tau_a(a,u) = \begin{cases} \tau_{\text{act}}(0.5 + 1.5a); & u > a \\ \tau_{\text{deact}}/(0.5 + 1.5a); & u \leq a \end{cases} \tag{3.2}$$

where τ_{act} is the activation time constant and τ_{deact} is the deactivation time constant. This relationship predicts that the activation slows as activation level increases due to less efficient

calcium release and diffusion. Similarly, the deactivation slows when muscle activation decreases [48].

3.2.2. HILL-TYPE MODEL OF MUSCLE–TENDON DYNAMICS

Musculoskeletal models are actuated by muscle–tendon units, each of which can be represented as a contractile element in series with a tendon [8]. A Hill-type model is used to characterize the contraction dynamics of muscle. This model represents muscles and tendons with simple elements; the biological complexities are distilled into the parameters and dimensionless curves that define the dynamics of these elements. It consists of three components: a contractile element (CE), a parallel element (PE), and a series element (see Figure 3.4). The generated muscle force is a function of three variables: the activation (a), the normalized length of the muscle fiber ($\tilde{\ell}^M$), and the normalized velocity of the muscle fiber ($\tilde{v}^M$). The tendon length below which the tendon produces zero force is called the tendon slack length (l_s^T). The functions that describe the muscle fiber force as a function of its length are called the active-force–length curve $f^L(\tilde{\ell}^M)$ for the contractile element and the passive-force–length curve $f^{PE}(\tilde{\ell}^M)$ for the parallel element.

During non-isometric contractions, the force developed by muscle varies nonlinearly with its rate of lengthening, which is represented by the force–velocity curve $f^V(\tilde{v}^M)$. Force is also developed when muscle is stretched beyond a threshold length, regardless of whether the muscle is activated, which is represented by the passive-force–length curve $f^{PE}(\tilde{\ell}^M)$. Muscle force (f^M) is computed using these curves as follows [8, 67]:

$$f^M = f_o^M \left[a\, f^L\left(\tilde{\ell}^M\right) f^V(\tilde{v}^M) + f^{PE}(\tilde{\ell}^M)\right] \tag{3.3}$$

where a is the muscle activation and f_o^M is the peak isometric muscle force.

Muscle attaches to bone through tendon. Since a long tendon may stretch appreciably beyond its slack length (l_s^T) when under tension, tendon is modelled as a nonlinear elastic element developing force according to the tendon-force–length curve $f^T(\tilde{\ell}^T)$. Muscle fibers attach to tendon at a pennation angle (α), scaling the force they transmit to the tendon. If the tendon is assumed to be elastic and the mass of the muscle is assumed to be negligible, then the muscle–tendon force equilibrium equation (i.e., $f^M \cos\alpha - f^T = 0$) is described as follows [8, 67]:

$$f_o^M \left[a\, f^L\left(\tilde{\ell}^M\right) f^V(\tilde{v}^M) + f^{PE}\left(\tilde{\ell}^M\right) \right] \cos\alpha - f_o^M\, f^T\left(\tilde{\ell}^T\right) = 0 \tag{3.4}$$

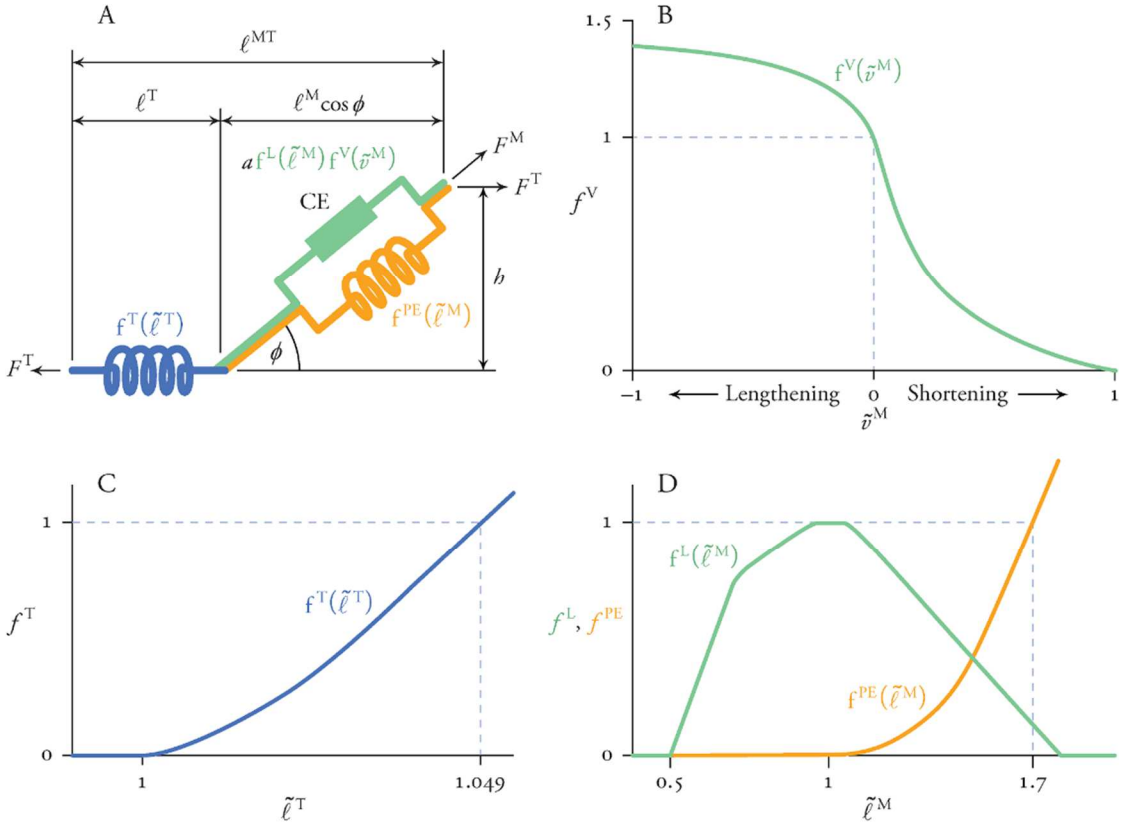

Figure 3.4. Schematic of a typical Hill-type muscle–tendon model (A) and the corresponding generic, dimensionless curves that describe the dynamics of its three components: the force–velocity curve (B), the tendon force–length curve (C), and the active and passive force–length curves (D) [8]. Image © 2020 David Delp; used with permission.

3.3. EXPERIMENTAL MOTION DATA

This study uses a publicly available dataset of 3D walking kinematics and ground reaction forces from elderly adults [42]. This dataset was collected using a motion capture system to record the kinematics and kinetics of participants during overground walking (i.e. not on a treadmill) at a comfortable pace. The data were collected from 24 young adults and 18 older adults, all of whom were free of lower-extremity injuries and orthopedic or neurologic diseases that could influence their gait patterns [42]. A motion capture system (Raptor-4; Motion Analysis Corporation) with 12 cameras and five force plates was used. The gait data from 10 of the older adult participants between 60 and 84 years of age (see Table 3.1) was used in this study. These participants were selected because most age-related gait changes appear after 60 years of age [10].

Participant identification number	Age (years)	Mass (kg)	Height (cm)	Sex	BMI (kg/m^2)	Gait speed (m/s)
S29	71	65.35	175.0	Male	21.33	1.46
S31	63	46.05	149.2	Female	20.68	1.12
S32	61	70.55	149.7	Female	31.48	1.42
S33	63	72.25	172.3	Male	24.33	1.24
S34	62	70.50	164.5	Male	26.06	0.99
S36	63	73.10	174.3	Male	24.06	1.38
S37	73	79.65	168.2	Male	28.15	1.12
S39	84	66.35	155.5	Male	27.43	0.98
S40	68	49.20	147.0	Female	22.76	1.34
S42	63	59.85	161.2	Female	23.03	0.95

Table 3.1. Data for each subject in our simulation study [42]. The last column indicates the gait speed selected by each subject when instructed to walk at a comfortable pace.

The experimental data required processing before OpenSim simulations could be generated. Twenty-eight retroreflective optical markers were placed in anatomical locations on the lower body of each participant [42]. The data were provided in the Coordinate 3D (C3D) file format, a standard format for experimental motion capture data. OpenSim requires marker trajectories to be specified in the Track Row Column (TRC) file format and ground reaction data in the motion (MOT) or OpenSim storage (STO) format [43]. The original C3D files were converted into formats accepted by OpenSim using the c3dExport.m and osimC3D.m MATLAB scripts that are provided with the OpenSim software. The OpenSim coordinate system defines the X-axis to be directed forward, the Y-axis upward, and the Z-axis pointing to the model's right (see Figure 3.5), but the motion data used in this study were collected using a different coordinate system, with the X-axis forward, the Y-axis pointing to the left, and the Z-axis upward. Thus, the data were rotated by 90 degrees about the X-axis using the osimC3D.m MATLAB script. The "Preview Experimental Data" function was used in the OpenSim GUI to visualize the marker and force data and confirm that this transformation was applied correctly.

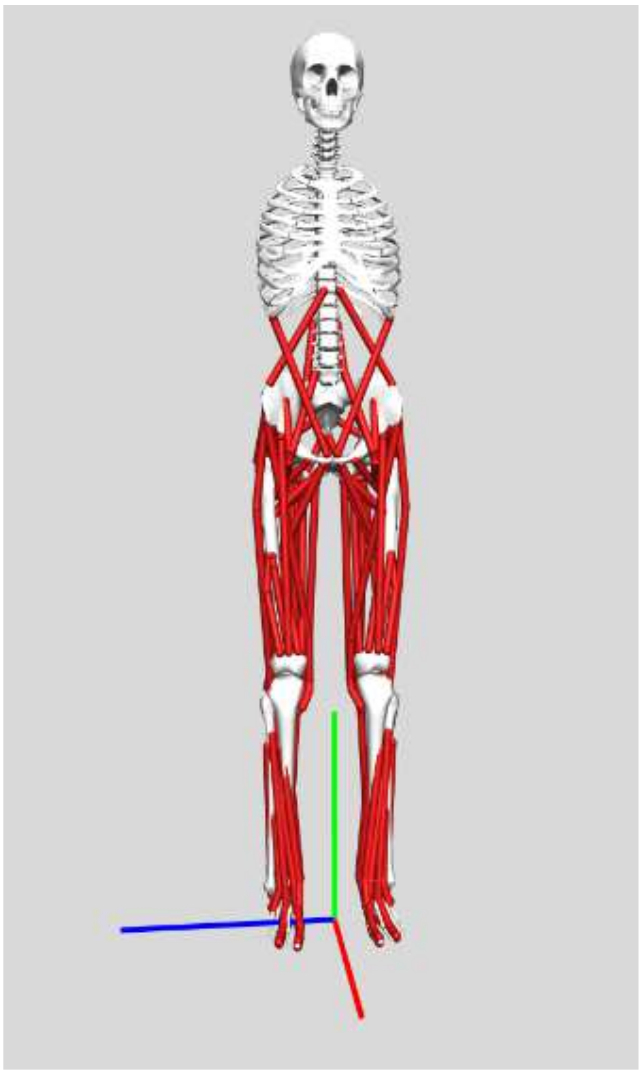

Figure 3.5. Global coordinate system in OpenSim with X directed forward (red line on the ground), Y directed upward (green line), and Z directed to the model's right (blue line).

3.4. SIMULATION WORKFLOW

OpenSim provides Tools to calibrate generic models based on subject-specific data, to perform inverse kinematic and inverse dynamic analyses, and to generate muscle-driven simulations [38]. The OpenSim workflow that was used in this study is shown in Figure 3.6 and described in detail below.

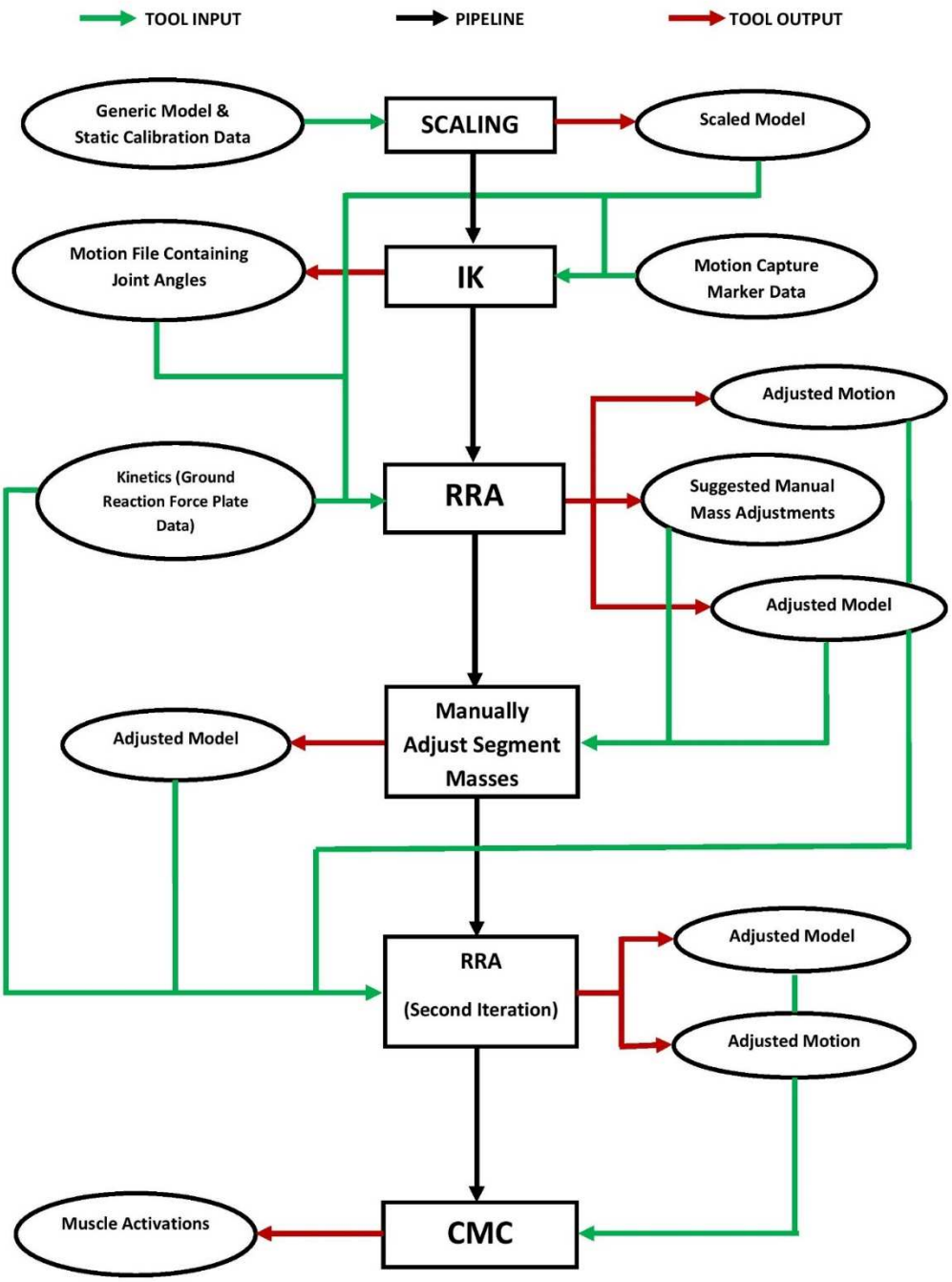

Figure 3.6. The OpenSim simulation workflow used in this study. The black arrows indicate the sequence in which the OpenSim Tools were run; the green and red arrows indicate, respectively, the inputs to and outputs from each Tool.

The first step in the simulation workflow was scaling the generic Gait2392 model for each subject so that it matched the subject's dimensions. The model was scaled using the 3D coordinates

of the 28 experimental markers during a “static calibration trial,” a single frame of motion capture data that was collected with the subject standing in a neutral position. These data were obtained from the public dataset provided by Fukuchi et al. [42]. The optical markers were assigned and “measurement sets” were defined using the Scale Tool. A measurement set contains pairs of experimental markers, the distances between which are used to scale the dimensions of each body segment of the model [40, 44, 45]. The Gait2392 model that is provided with OpenSim 4.0 included all the markers required to track the experimental data in the Fukuchi et al. [42] dataset. The markers on the models were adjusted to match the experimental marker locations. Model markers were weighted according to how closely the model and experimental marker locations were expected to match. Marker weights determine how well each model marker will track the corresponding experimental marker during the inverse kinematic analysis. A larger weight assigned to a marker will result in less marker error, or a smaller distance between the model and experimental markers. In the Scale Tool, the “Preserve mass distribution during scale” option was selected, meaning that the total mass of the generic model was scaled so that it equals the mass of the subject while preserving the relative masses of the model’s body segments [47]. Table 3.2 lists the 28 anatomical markers that were used to determine the position and orientation of the body segments during the walking trials. The root mean square (RMS) marker error and maximum error were obtained from the Messages window in the OpenSim GUI after running the Scale Tool. Each of the scaled models had an RMS marker error less than 1 cm and a maximum marker error less than 2 cm for all markers placed on bony landmarks, meeting the recommendations suggested by Hicks et al. [41]. Scaling resulted in a set of 10 musculoskeletal models with the dimensions of the study participants.

	Marker Label	Anatomical Location
1	R.ASIS	Right anterior superior iliac spine
2	L.ASIS	Left anterior superior iliac spine
3	R.PSIS	Right posterior superior iliac spine
4	L.PSIS	Left posterior superior iliac spine
5	R.Iliac.Crest	Uppermost margin of the right iliac crest
6	L.Iliac.Crest	Uppermost margin of the left iliac crest
7	R.Heel.Bottom	Aspect of the Achilles tendon insertion on the right calcaneous
8	L.Heel.Bottom	Aspect of the Achilles tendon insertion on the left calcaneous
9	R.GTR	Most lateral prominence of the right greater trochanter
10	R.Knee	Most lateral prominence of the right lateral femoral epicondyle
11	R.Knee.Medial	Most medial prominence of the right lateral femoral epicondyle
12	R.HF	Proximal tip of the head of the right fibula
13	R.TT	Most anterior border of the right tibial tuberosity
14	R.Ankle	Lateral prominence of the right lateral malleolus
15	R.Ankle.Medial	Most medial prominence of the right medial malleolus
16	R.MT1	Dorsal margin of the right 1st metatarsal head
17	R.MT5	Dorsal margin of the right 5th metatarsal head
18	R.MT2	Dorsal margin of the right 2nd metatarsal head
19	L.GTR	Most lateral prominence of the left greater trochanter
20	L.Knee	Most lateral prominence of the left lateral femoral epicondyle
21	L.Knee.Medial	Most medial prominence of the left lateral femoral epicondyle
22	L.HF	Proximal tip of the head of the left fibula
23	L.TT	Most anterior border of the left tibial tuberosity
24	L.Ankle	Lateral prominence of the left lateral malleolus
25	L.Ankle.Medial	Most medial prominence of the left medial malleolus
26	L.MT1	Dorsal margin of the left 1st metatarsal head
27	L.MT5	Dorsal margin of the left 5th metatarsal head
28	L.MT2	Dorsal margin of the left 2nd metatarsal head

Table 3.2. Anatomical locations of the 28 optical markers used to track the position and orientation of each body segment during walking trials [42].

In addition to adjusting the dimensions of the model, several modifications were made to the model's dynamic properties to reflect age-related changes in muscle mechanics. The adjustments for elderly individuals were made to the Gait2392 model based on the recommendations from Thelen [48]. In this study, the following adjustments were made: the muscle isometric force was decreased by 30% to account for the loss of muscle mass and strength due to aging, muscle deactivation time was increased by 20%, maximum contraction velocity was decreased by 20%, the passive stress–strain relation of the muscle was adjusted to account for the relative increase in passive stiffness, and the maximum normalized force during eccentric contraction was increased from 1.4 for younger adults to 1.8 for older adults [48].

The scaled models were then used with OpenSim's Inverse Kinematics (IK) Tool to compute the motion of each body segment from the motion capture marker data. The IK Tool solves a least-squares problem that minimizes the distances between the experimental marker locations and the locations of the corresponding model markers [49]:

$$\min_{q}\left[\sum_{i\in\text{markers}} w_i\|{x_i}^{\text{exp}} - x_i(q)\|^2 + \sum_{j\in\text{unprescribed coords}} w_j\left({q_j}^{\text{exp}} - q_j\right)^2\right] \tag{3.5}$$

where q is the vector of generalized coordinates being computed, ${x_i}^{\text{exp}}$ is the location of experimental marker i, $x_i(q)$ is the location of the corresponding model marker (which depends on the coordinate values), and ${q_j}^{\text{exp}}$ is the experimental value for coordinate j. The marker weights (w_i) and coordinate weights (w_j) are specified in the IK setup files.

The IK Tool uses motion capture data to estimate the joint angles of the subject at each time frame of the trial, again by minimizing the error between the model and experimental markers (but now where the model dimensions are constant). The scaled model and motion capture data files

were used as inputs to the IK Tool. OpenSim generated a motion file containing the trajectories of the model's coordinates (joint angles). The maximum marker error and RMS error were reported in the Messages window in the OpenSim GUI and were less than 2 cm, as recommended in the literature [41, 49]. The IK results compared favorably to the experimental kinematics collected by Fukuchi et al. [42] as well as other experimental kinematics reported in the literature [2, 10].

The Residual Reduction Algorithm (RRA) Tool makes slight changes to the body segment masses in the model and to the joint angles computed by the IK Tool to minimize the "residual forces," which are the fictitious forces that actuate the three translational degrees of freedom between the pelvis and the ground. These fictitious forces represent the error between the kinematic and dynamic experimental data and must be minimized. Typically, these errors occur due to modelling assumptions, noise, and other errors from motion capture data which lead to dynamic inconsistency. The ground reaction forces and accelerations estimated from measured marker kinematics for a subject do not satisfy Newton's Second Law ($F = ma$). Thus, the residuals amount to adding a new force to the equation that accounts for inconsistencies [50]:

$$F + F_{\text{residual}} = ma \tag{3.6}$$

The RRA Tool requires one to filter the kinematic data because differentiation amplifies the high-frequency noise that these data typically contain. One way to avoid noise is to smooth the data with a low-pass filter, which removes high-frequency content. The frequency range of interest depends on the activity being studied, thus so does the appropriate filter cut-off frequency. For example, we may be interested in frequencies up to about 3 Hz for studying posture, 6 Hz for studying walking, and 10–15 Hz for studying running [8]. Therefore, we filtered the kinematics at 6 Hz in this work; an updated model with a new body COM was then obtained. The ground reaction force data were low-pass filtered with a cut-off frequency of 8 Hz. The RRA Tool differentiates

the joint angles with respect to time to estimate joint angular velocities and accelerations, which are used with measurements of the external forces applied to the body to estimate joint moments [8]. An "external loads" file was created using the ground reaction force (.mot) file, and the forces measured by each force plate were applied to either the left or right calcaneus (depending on the foot used by the participant to step on each plate). Slight changes were made to the model and motion to generate adjusted models for each subject using the RRA Tool. This step was iterative, as OpenSim provides suggestions for more drastic mass changes that must be made to the model manually between iterations until the adjustments suggested by RRA were small. The average value of F_y (vertical component of the residual actuator force) was used to compute the recommended mass changes for all the body segments [50]. The desired mass change (Δm) was calculated as follows:

$$\Delta m = F_y / g \tag{3.7}$$

where g= -9.81 m/s^2. This mass change was then distributed among the body segments such that the ratios of their masses remained constant. The average value for each residual actuator (force or torque) was computed by OpenSim. The average residual torques were used to adjust the torso mass center to correct for excessive bending of the model, likely due to inaccuracies in the mass distribution and geometry of the torso [50]. A new model file was created and the optimized motion with reduced residual forces was used in the Computed Muscle Control (CMC) Tool, described next.

The CMC Tool computes the muscle excitations that are necessary to drive the musculoskeletal model through a specified motion. CMC uses a combination of proportional–derivative (PD) control and static optimization to solve the muscle redundancy problem [8], seeking to minimize the sum of squared muscle activations. The CMC algorithm first computes

the joint accelerations required to drive the model through the experimental motion. The desired accelerations are computed using the following PD control law [49]:

$$\ddot{q}\,(t\,+\,T) = \ddot{q}_{\exp}(t\,+\,T) + \,k_v\left[\dot{q}_{\exp}\,(t)\,-\,\dot{q}\,(t)\right] + k_p\,[q_{\exp}(t)\,-\,q(t)] \tag{3.8}$$

where k_v and k_p are feedback gains for the velocity and position errors, respectively. The CMC algorithm then uses static optimization to compute the muscle control signals (muscle excitations) that are required to achieve the desired accelerations (i.e., to track the experimental motion). The last step of CMC is to use these controls to perform a forward dynamic simulation, advancing the model forward in time. The CMC Tool repeats these steps until it reaches the end of the provided motion [48]. The CMC Tool was used to generate muscle-driven simulations of the 10 overground trials using the RRA-adjusted model and the RRA-adjusted kinematics. The CMC look-ahead window (the duration of the forward dynamic simulations referred to above) was set to 5 ms from the default value of 10 ms to reduce the noise present in some results. The CMC simulation results were evaluated based on threshold values reported in the literature. The peak residual force was less than 25 N, the peak residual torque was less than 75 N·m, and the peak reserve torque was less than 50 N·m for all 10 subject trials, as recommended by Hicks et al. [41]. The results obtained did not include the initial double-support phase of the gait cycle, since the database contained ground reaction force data from only two consecutive force plates. To analyze one full gait cycle, the second double-support phase in each trial was duplicated, mirrored, and added at the beginning of the trial to represent the first double-support phase.

3.5. SIMULATING ASSISTIVE DEVICES

In this section, the process used to generate simulations of device-assisted walking for 10 subjects using OpenSim is described. This study aimed to investigate how ideal and torque-limited assistive devices affect the metabolic cost of healthy elderly walking.

3.5.1. IDEAL ASSISTANCE

To seek insight into the biomechanical and energetic effects of assistive devices for elderly walking, ideal devices were added bilaterally to assist the hip flexion/extension, knee flexion/extension, ankle plantarflexion/dorsiflexion, or hip abduction/adduction degrees of freedom in the OpenSim models. Each assistive device was modelled as a massless, lossless actuator that applied torque directly to the joint. Neither the magnitude nor the rate of assistive torque were limited, allowing each device to apply the ideal amount of torque to each joint [29]. This simulation strategy provides an approximation of the best possible effectiveness of an assistive device at reducing the metabolic energy consumed by the wearer. The ideal devices were added by increasing the strength of the model's reserve actuators at the hips, knees or ankles of the elderly models. Typically, the reserve actuators compensate for brief periods of muscle weakness in the model by applying additional joint torques. Specifically, the reserve actuators activate if the muscles are unable to generate the necessary joint moments to track the experimental data. Typically, the reserve torques are minimized to prevent the model from recruiting these actuators if they are not required, since reserve actuators are not present in the biological system.

CMC simulations were generated for all subjects by applying the experimentally measured ground reaction forces and tracking the RRA-adjusted kinematics. The following instantaneous objective function is used by CMC to balance the recruitment of reserve actuators with the recruitment of muscles [29]:

$$J(a,\tau) = \sum_{i=1}^{\text{nMuscles}} a_i^2 + \sum_{j=1}^{\text{nReserves}} \left(\frac{\tau_j}{w_j}\right)^2 \quad (3.9)$$

where nMuscles and nReserves refer to the number of musculotendon and reserve actuators in the model, a_i represents the instantaneous activation of the ith muscle, τ_j is the instantaneous torque applied by the jth reserve actuator, and w_j is the constant weighting factor that scales the penalty of recruiting the jth reserve actuator [29]. The weighting factors were set to 1 N·m during the original (unassisted) simulations, to penalize the solution by the square of the torque generated by the reserve actuator, as shown in Eq (3.9). Because the muscle activations a_i are between 0 and 1, the peak reserve actuator torques were very small. To simulate the ideal assistive devices, the corresponding weighting factors were increased to 10^6 N·m, which results in a negligible penalty in the objective function when a reserve actuator is recruited. In this way, the CMC simulations were used to predict the forces that would be generated by the muscles when using an ideally designed assistive device. CMC simulations were generated for each of the 10 elderly subjects when unassisted and in each assistance scenario.

The energy consumed by each muscle (metabolic cost) was computed using the Umberger2010MuscleMetabolicsProbe in OpenSim. This OpenSim component implements the model proposed by Umberger [51] and modified by Uchida et al. [29, 52]. The Probes were added to each musculoskeletal model (programmatically in Python) to calculate the metabolic power consumed by each of the lower-extremity muscles during the simulation. The energy consumed by lower-extremity muscles was used to establish metabolic cost because relatively little energy is expended by other muscles in the body during walking [8].

The average metabolic power consumed by each muscle was calculated by integrating the instantaneous power consumption over one gait cycle (resulting in the total energy consumed, in

Joules) and then dividing by the gait cycle duration to obtain average power (in Watts). The average power was then summed across all 86 lower-limb muscles in the model. Finally, the total average metabolic power was divided by the mass of the subject, resulting in the average metabolic power consumed per kilogram (W/kg). Normalizing by subject mass facilitates comparison between subjects of different mass. The calculated metabolic cost of walking, C_{calc}, is determined in W/kg as follows [52]:

$$C_{\text{calc}} = \frac{1}{Tm} \sum_{i=1}^{N_{\text{mus}}} \int_0^T \dot{E}_i(t)\, dt \tag{3.10}$$

where T denotes the motion duration, m is the participant's mass, N_{mus} is the number of muscles, and $\dot{E}_i(t)$ is the rate of energy consumption for muscle i (in Watts). The performance of each ideal assistive device was evaluated by comparing the average metabolic power consumed in the assisted scenario with that consumed in the unassisted scenario. This analysis was performed for each subject and ideal assistance scenario. The mean and standard deviation of the metabolic cost savings were computed for each device for comparison.

3.5.2. TORQUE-LIMITED ASSISTANCE

Torque-limited assistance was simulated to investigate a non-ideal aspect of assistive devices, specifically the metabolic savings when the maximum device torque was limited to 25%, 50%, or 75% of the maximum torque magnitude from the ideal assistance simulations. Motors (actuators) were added to the "actuators" configuration file. They were added bilaterally at one of the following four coordinates: hip flexion/extension, hip abduction/adduction, knee flexion/extension or ankle plantarflexion/dorsiflexion. The "control constraints" configuration file was modified. The maximum possible torque of the reserve actuators was set to a percentage of the maximum

absolute value of the torque that the ideal actuators generated (at that coordinate and for that subject), the limit being either 25%, 50%, or 75% of the maximum ideal torque. For example, the control constraints for the 25%-torque-limited simulations will be identical to the torque generated by the ideal device if the control signal (between 0 and 1) is less than or equal to 0.25. The control constraints file specifies minimum and maximum bounds for control values at each time point; this file was used in the CMC Tool to generate torque-limited simulations. Simulations were run with the limit set to 100% to verify the simulation framework: the metabolic cost computed from these simulations was confirmed to be the same as the metabolic cost when using the ideal actuators.

3.6. STATISTICAL ANALYSIS

The analysis of variance (ANOVA) test was performed to determine the significant main effect between the metabolic savings of different devices. The paired t-test was performed as a post-hoc to determine which assistance strategy is best (hip flexion/extension, hip abduction/adduction, knee flexion/extension or ankle plantarflexion/dorsiflexion) and whether there are any apparent differences between ideal and torque-limited assistance. ANOVA and paired t-tests between each assistance scenario at each joint were performed with a significance level of $\alpha = 0.001$. In this study, the null hypothesis states that there is no significant difference between the ideal and torque-limited devices. Conventionally, $p<0.001$ is referred to as being statistically highly significant because it provides very strong evidence against the null hypothesis [68]. The statistical tests were performed using Python.

CHAPTER 4: RESULTS AND DISCUSSION

This chapter describes the results of simulations of unassisted, healthy elderly walking, and healthy elderly walking with hypothetical ideal and torque-limited assistive devices. Experimental data from the literature were used to validate the results of the unassisted simulations. All simulations were performed using OpenSim 4.0. Details about the generation and verification of our simulation results can be found in Appendix A.

4.1. VALIDATION OF UNASSISTED SIMULATIONS

Before simulating hypothetical ideal and torque-limited assistive devices, the results of the unassisted simulations were validated to ensure they captured the known relationship between metabolic cost and walking speed. The experimental data reported by Rathkey and Wall-Scheffler [53] were used to validate our results. Rathkey and Wall-Scheffler computed the average metabolic cost of 9 young adult men walking on a treadmill. Figure 4.1 shows the metabolic power, averaged over one gait cycle and normalized by subject mass (W/kg), computed from the simulations of 10 elderly subjects and the measurements reported by Rathkey and Wall-Scheffler for young adults over a range of walking speeds (m/s). We observe the same trend in the simulations as in the experimental data: metabolic cost increases as walking speed increases. The calculations of metabolic cost are clearly higher than the experimental data, likely due to differences in age, body mass index (BMI), strength, and other variables between our subjects and theirs, as well as approximations in our musculoskeletal models. However, in this study we are interested in comparing the predicted reduction in metabolic cost when various assistive devices are simulated rather than comparing the absolute values of the metabolic cost predictions; thus, we consider validation of the trend shown in Figure 4.1 to be acceptable. In fact, one would indeed expect

metabolic power consumption to be higher in elderly individuals since, on average, they have lower muscle mass and strength [2].

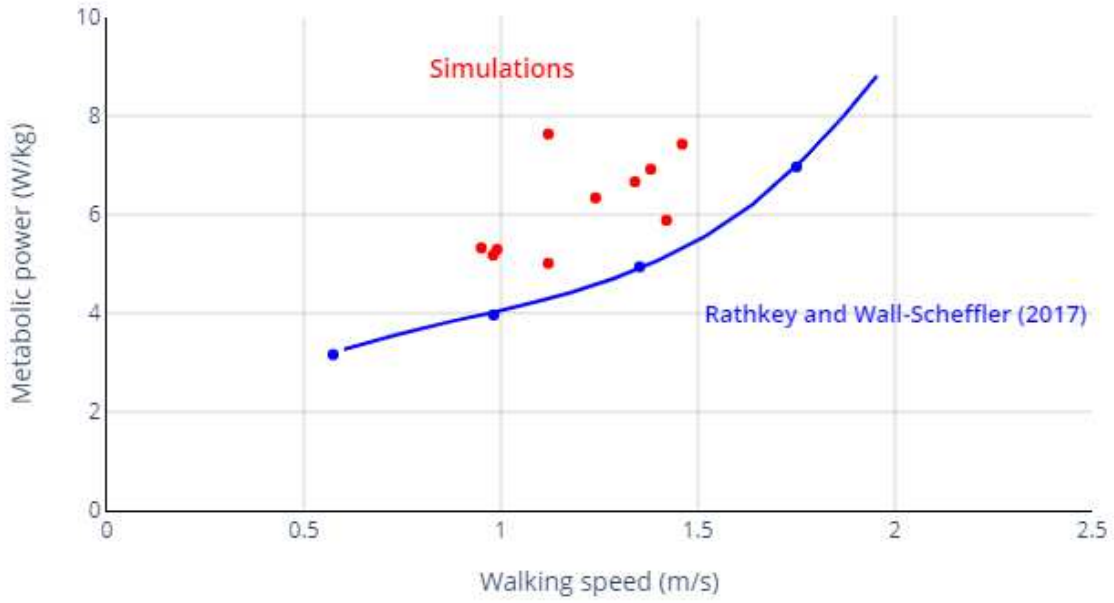

Figure 4.1. Metabolic power computed from unassisted simulations of 10 elderly subjects walking (red) and experimental data collected from young adult men (average over 9 subjects; blue) reported by Rathkey and Wall-Scheffler [53]. All data were normalized by subject mass.

The average metabolic cost from the unassisted simulations of 10 elderly subjects walking, computed over one gait cycle, is shown for each subject in Table 4.1. Based on the results, subject 31 appears to be an outlier with a metabolic cost of 7.63 W/kg at a walking speed 1.12 m/s (also see Figure 4.1). This subject has very low mass (46.05 kg) and thus the parameters in the model (e.g., the optimal muscle fiber lengths, tendon slack lengths, and 3D paths of each muscle) are likely poor approximations for this subject. Note that the same adjustments were applied to the muscle model parameters for all subjects, according to the adjustments recommended by Thelen [48] (described in Section 3.4). These adjustments do not consider several potentially important differences among subjects, such as BMI (which may correlate with the maximum isometric force of a muscle), sex, age, and data from strength tests.

Participant identification number	Mass (kg)	Walking speed (m/s)	Metabolic cost (W/kg)
S29	65.35	1.46	7.42
S31	46.05	1.12	7.63
S32	70.55	1.42	5.88
S33	72.25	1.24	6.34
S34	70.50	0.99	5.29
S36	73.10	1.38	6.92
S37	79.65	1.12	5.01
S39	66.35	0.98	5.17
S40	49.20	1.34	6.66
S42	59.85	0.95	5.32

Table 4.1. Calculated metabolic cost for 10 elderly subjects during walking at a self-selected comfortable pace. Metabolic cost is computed as the average metabolic power consumed over time, normalized by subject mass.

4.2. METABOLIC SAVINGS WITH IDEAL ASSISTIVE DEVICES

To explore the relative effectiveness of assisting different joints in the lower limb, CMC simulations were generated using the data described above but where ideal assistive devices were added bilaterally to assist hip flexion/extension, hip abduction/adduction, knee flexion/extension or ankle plantarflexion/dorsiflexion. In total, 40 additional CMC simulations were generated for this analysis: one for each assistive device scenario for each of our 10 elderly subjects. A reduction in average metabolic power consumption was observed in all ideal assistance scenarios compared to the unassisted scenario. Figure 4.2 shows the reduction in average power expended by lower-limb muscles over one gait cycle, normalized by subject mass. Table 4.2 summarizes the metabolic cost computed for each subject in the unassisted and ideal assistance scenarios, and the percent reduction in metabolic cost obtained using each ideal assistive device.

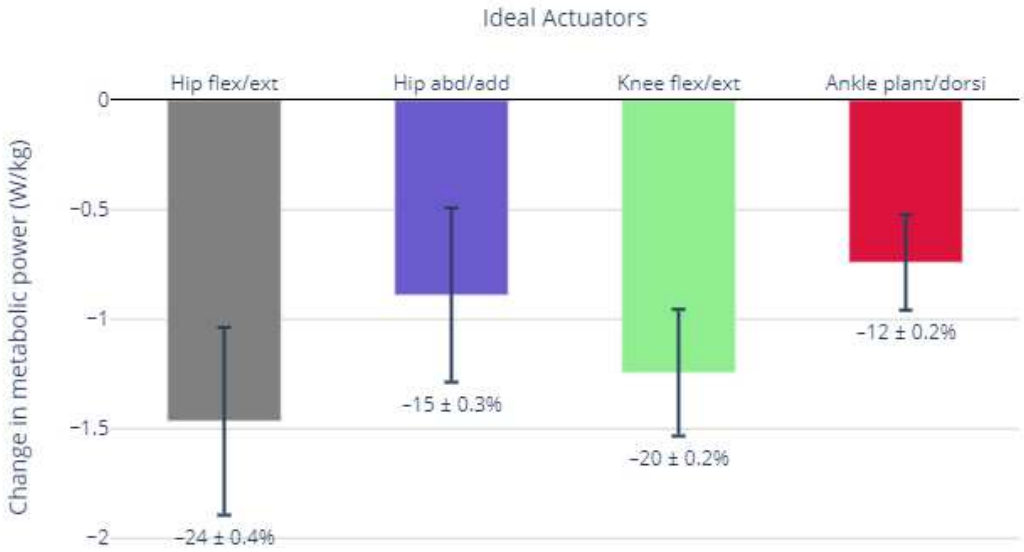

Figure 4.2. Metabolic savings with ideal hip flexion/extension (grey), hip abduction/adduction (purple), knee flexion/extension (green) and ankle plantarflexion/dorsiflexion (red) actuators. Mean and standard deviation of the savings are shown as columns and bars, respectively, and also labelled beneath each column as a percentage of the unassisted cost.

Subject	Metabolic cost when unassisted (W/kg)	Ideal hip flexion/extension actuators		Ideal hip abduction/adduction actuators		Ideal knee flexion/extension actuators		Ideal ankle plantarflexion/dorsiflexion actuators	
		cost (W/kg)	reduction (%)	cost (W/kg)	reduction (%)	cost (W/kg)	reduction (%)	cost (W/kg)	reduction (%)
S29	7.42	4.99	32.8	6.94	6.5	6.01	19.1	6.43	13.5
S31	7.63	6.13	19.7	6.55	14.1	6.04	20.7	6.53	14.3
S32	5.88	4.28	27.3	4.42	24.8	4.83	17.8	4.89	16.8
S33	6.34	5.00	21.1	5.75	9.2	4.92	22.3	5.63	11.2
S34	5.29	4.07	23.0	3.76	29.0	4.46	15.8	4.68	11.6
S36	6.92	5.11	26.1	6.14	11.1	5.41	21.7	6.34	8.3
S37	5.01	3.80	24.1	4.27	14.8	4.04	19.2	4.59	8.4
S39	5.17	3.83	25.9	4.66	9.8	4.11	20.5	4.57	11.6
S40	6.66	5.26	21.0	6.11	8.2	5.04	24.3	5.91	11.3
S42	5.32	4.50	15.4	4.13	22.4	4.31	18.9	4.67	12.1

Table 4.2. Metabolic cost of unassisted and assisted scenarios (W/kg) and, for assisted scenarios, the reduction in metabolic cost relative to unassisted for each subject.

Among the four ideal assistance scenarios we investigated, the hip flexion/extension device resulted in the greatest reduction in metabolic cost (24% on average), while the ankle

plantarflexion/dorsiflexion device resulted in a reduction of only 12% (see Figure 4.2). The most beneficial strategy for assisting elderly gait may be hip flexion/extension assistance. As shown in Figure 4.2, metabolic power consumption decreased by 20% when assisting the knee (average over 10 elderly subjects) and by 15% when assisting hip abduction/adduction. Most experimental studies focus on ankle assistance; however, our findings suggest that greater metabolic savings may be achieved by assisting the hip or knee. These results agree with those reported by Dembia et al. [6] for younger adults and suggest a direction for future development of exoskeletons to assist elderly gait.

Table 4.3 shows the ANOVA test results for ideal assistive devices, and Table 4.4 shows the results of paired t-tests to determine whether the apparent differences shown in Figure 4.2 are in fact statistically significant. The results of these statistical analyses showed no significant difference between hip flexion/extension vs. hip abduction/adduction, hip flexion/extension vs. knee flexion/extension, hip abduction/adduction vs. knee flexion/extension, and hip abduction/adduction vs. ankle plantarflexion/dorsiflexion devices (highlighted in Table 4.4). A greater reduction in metabolic power during ideal hip flexion/extension assistance agrees with the results of Dembia et al. [6] for younger adults walking. However, the results differ somewhat from experimental studies evaluating the effectiveness of WAEs with elderly individuals. A powered hip exoskeleton was designed by Seo et al. [54] to assist hip flexion and extension during elderly gait. The device was tested on healthy, elderly participants (N = 30) and resulted in only a 7% reduction in metabolic cost. Ding et al. [55] reported a metabolic savings of 17.4% when heathy, young adults walked with a hip exoskeleton (N = 8), and Lim et al. [56] reported a 19.4% reduction in metabolic cost with a hip assistive device when tested on young adults (N = 6). The simulations used assistive devices that were massless and able to provide large amounts of torque to the joints;

thus, it is reasonable to expect that experimental trials would result in smaller metabolic cost reductions (discussed further in Chapter 5).

Groups	ANOVA (p-value)
Hip flexion/extension vs. Hip abduction/adduction	0.006
Hip flexion/extension vs. Knee flexion/extension	0.193
Hip flexion/extension vs. Ankle plantarflexion/dorsiflexion	0.0001*
Hip abduction/adduction vs. Knee flexion/extension	0.035
Hip abduction/adduction vs. Ankle plantarflexion/dorsiflexion	0.0001*
Knee flexion/extension vs. Ankle plantarflexion/dorsiflexion	0.0003*

Table 4.3. Results of ANOVA test between metabolic savings of four ideal assistive devices. Statistically significant differences are denoted by an asterisk (*).

	Hip flexion/extension	**Hip abduction/adduction**	**Knee flexion/extension**	**Ankle plantarflexion/dorsiflexion**
Hip flexion/extension	—			
Hip abduction/adduction	0.0258	—		
Knee flexion/extension	0.1015	0.0965	—	
Ankle plantarflexion/dorsiflexion	0.0001*	0.2934	0.0002*	—

Table 4.4. Results of paired t-tests between metabolic savings of four ideal assistive devices. Statistically significant differences are denoted by an asterisk (*).

4.3. CHANGES IN MUSCLE COORDINATION WITH IDEAL ASSISTANCE

Our simulations predict several changes in muscle activity when assistance is added, suggesting some of the biological effects of assistive devices. The metabolic power consumed by a muscle depends primarily on its activation and the composition, length and velocity of its fibers [28, 29]. Figure 4.3 illustrates the major muscles in the human lower limb. We observed large reductions in the metabolic power consumed by uniarticular muscles when an ideal actuator was added at the joint spanned by the muscle (see Figure 4.4). For example, the iliopsoas showed a substantial reduction in metabolic power consumption when ideal hip flexion/extension actuators were added: average metabolic power decreased from 0.774 W/kg to 0.090 W/kg, or approximately 88%. The glutei muscles showed a decrease in average metabolic power from 1.640 W/kg to 0.563 W/kg when the ideal hip abduction/adduction actuators were added (see Table 4.3). A combined reduction of 70% was observed in the biceps femoris short head and vasti muscles when assisting knee flexion/extension, and a combined 88% reduction was observed in the soleus and tibialis anterior muscles when the ideal ankle plantarflexion/dorsiflexion actuators were added. Note that, while substantial, these reductions should theoretically have been 100% since it would have been "free" for the actuators to generate the torques that were still generated by these uniarticular muscles, but the optimizer used by the CMC Tool did not find these solutions. However, the metabolic power consumed by these muscles was still relatively low, as would be expected. For example, the vasti and biceps femoris short head have low metabolic cost relative to the other muscles (0.222 W/kg and 0.044 W/kg, respectively) when assisting knee flexion/extension.

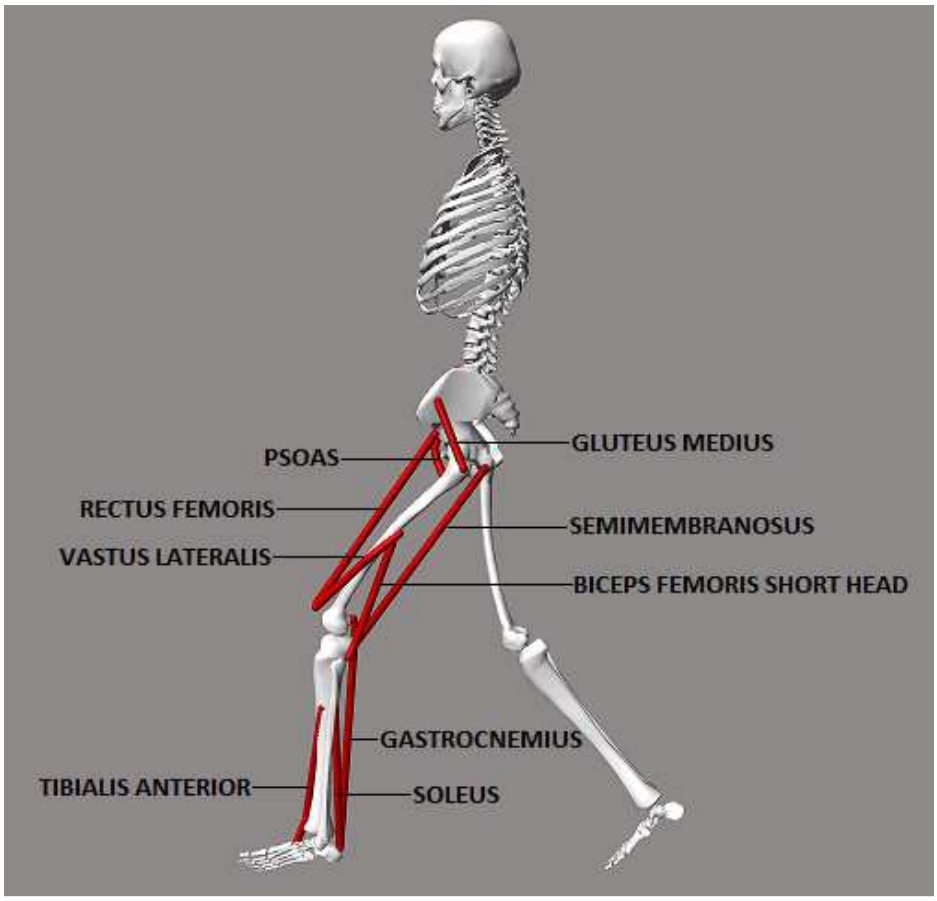

Figure 4.3. Major muscles in the human lower limb.

Muscle or group	Unassisted (W/kg)	With hip flexion/extension assistance (W/kg)	With hip abduction/adduction assistance (W/kg)	With knee flexion/extension assistance (W/kg)	With ankle plantarflexion/dorsiflexion assistance (W/kg)
Iliopsoas	0.774	0.090	0.654	0.489	0.773
Glutei	1.640	1.447	0.563	1.639	1.649
Rectus femoris	0.289	0.190	0.224	0.428	0.308
Biarticular hamstrings	0.662	0.568	1.017	0.453	0.700
Vasti	0.477	0.386	0.637	0.222	0.490
Biceps femoris short head	0.414	0.308	0.318	0.044	0.426
Gastrocnemii	0.489	0.419	0.442	0.261	0.432
Tibialis anterior	0.245	0.234	0.239	0.224	0.027
Soleus	0.444	0.456	0.453	0.481	0.056
Other muscles	0.734	0.604	0.731	0.683	0.567
Total	**6.169**	**4.703**	**5.278**	**4.924**	**5.428**

Table 4.5. Metabolic power expended by each muscle or muscle group when unassisted and when assisted by ideal devices. Data are averaged over the gait cycle, averaged over 10 elderly subjects, and normalized by subject mass.

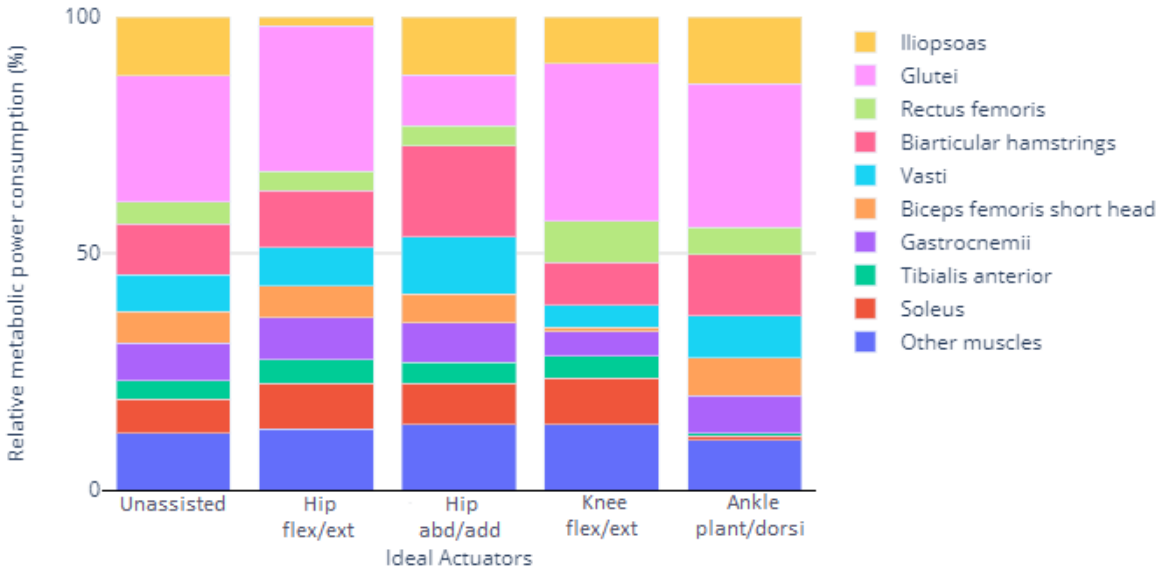

Figure 4.4. Relative metabolic power consumed by each muscle or muscle group in the unassisted scenario (leftmost column) and when assisted by ideal hip flexion/extension (Hip flex/ext), hip abduction/adduction (Hip abd/add), knee flexion/extension (Knee flex/ext), or ankle plantarflexion/dorsiflexion (Ankle plant/dorsi; rightmost column) actuators.

Figures 4.5–4.8 show the activations of nine representative lower-extremity muscles in each ideal assistance scenario. Mean activations are shown for three uniarticular muscles on the posterior side of the leg (left column), three uniarticular muscles on the anterior side of the leg (right column), and three biarticular muscles (center column). A decrease in the activity of the psoas and gluteus medius was observed when assisting hip flexion/extension and abduction/adduction, respectively (Figures 4.5 and 4.6). The activation of the rectus femoris increased when assisting hip flexion/extension and knee flexion/extension to take advantage of its relatively high force-generating capacity (see Figures 4.5 and 4.7). A muscle fiber can generate more force when lengthening than when shortening [45] and the rectus femoris muscle fibers were lengthening during early swing while the fibers of the psoas (a uniarticular hip flexor muscle in the model) were shortening. A substantial decrease in activity was observed in the biceps femoris short head and vastus lateralis when assisting knee flexion/extension (Figure 4.7) because the knee moments generated by these (uniarticular) muscles when unassisted could be generated by the ideal actuator at negligible cost without affecting the muscle-generated moments at the other joints (see Eq (3.9) in Section 3.5.1). An increase in the activity of the vastus lateralis at the end of the gait cycle was observed when assisting knee flexion/extension (Figure 4.7), which should theoretically be low, but the OpenSim optimizer did not find a better solution. The soleus and tibialis anterior activations decreased dramatically throughout the gait cycle when assisting ankle plantarflexion/dorsiflexion (Figure 4.8) because these muscles can generate only ankle moments; the ideal actuator generated these moments at negligible cost and without affecting the muscle-generated moments at the knee or hip.

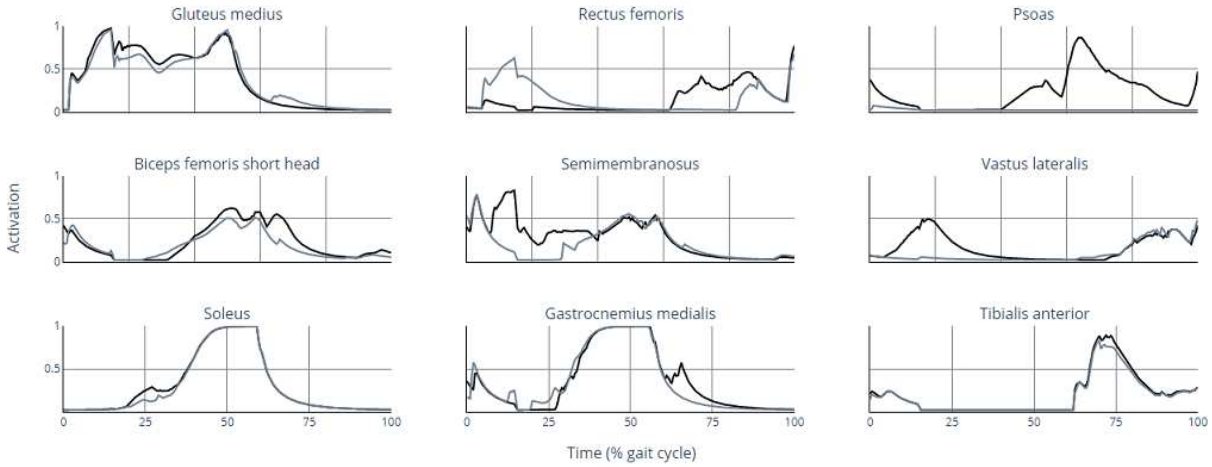

Figure 4.5. Activations of nine representative lower-extremity muscles when unassisted (black) and when assisting hip flexion/extension (grey).

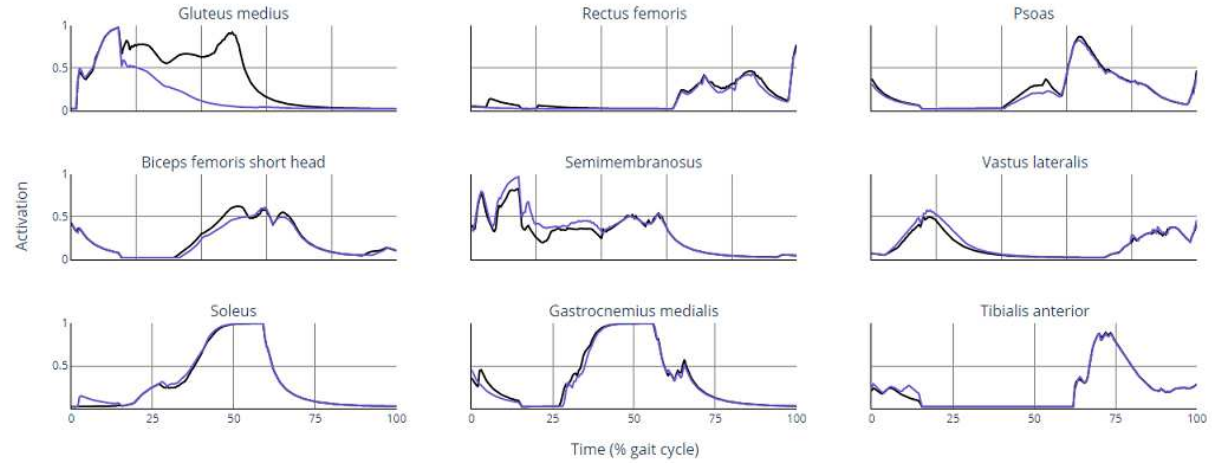

Figure 4.6. Activations of nine representative lower-extremity muscles when unassisted (black) and when assisting hip abduction/adduction (purple).

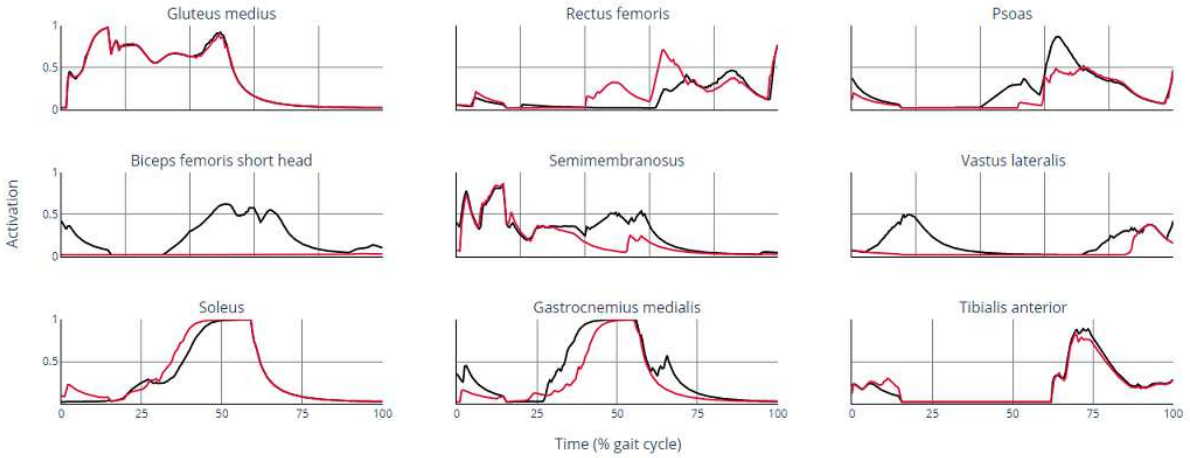

Figure 4.7. Activations of nine representative lower-extremity muscles when unassisted (black) and when assisting knee flexion/extension (red).

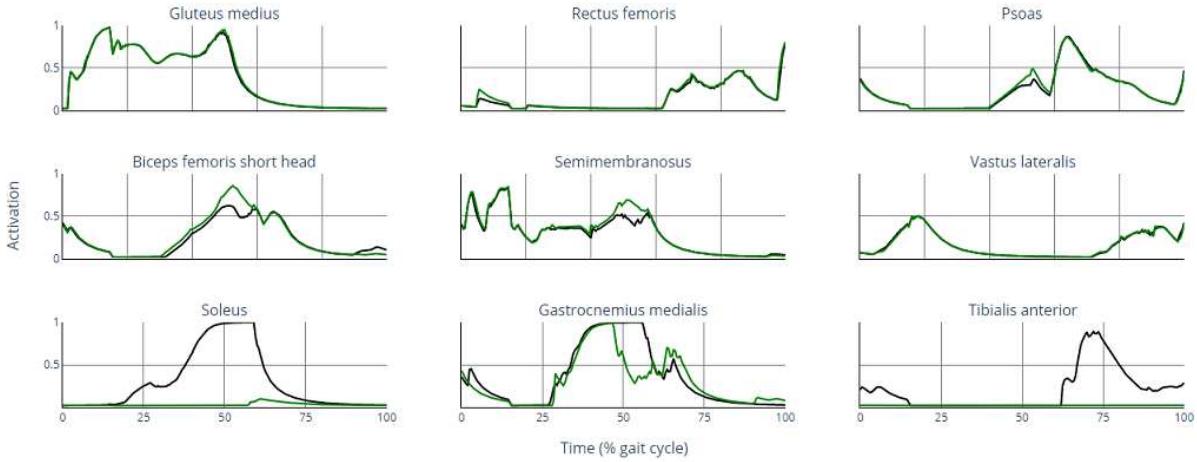

Figure 4.8. Activations of nine representative lower-extremity muscles when unassisted (black) and when assisting ankle plantarflexion/dorsiflexion (green).

4.4. TORQUE PROFILES OF IDEAL DEVICES

The torques generated by the ideal assistive devices in our simulations provide insight into the magnitude and timing of torques that may be beneficial in physical devices. Figures 4.9–4.12 show the torque generated by ideal hip flexion/extension, hip abduction/adduction, knee flexion/extension and ankle plantarflexion/dorsiflexion actuators, normalized by subject mass (N·m/kg). The results suggest that, although the ideal hip flexion/extension actuator reduced

average metabolic power more than the other ideal assistive devices we investigated, the maximum standard deviation (shaded region) of the actuator torque over the gait cycle (0.533 N·m/kg) was substantially greater for the hip flexion/extension actuator (Figure 4.9) than for the other devices. The maximum standard deviation was 0.368 N·m/kg for the hip abduction/adduction actuator (Figure 4.10), 0.386 N·m/kg for the knee flexion/extension actuator (Figure 4.11) and 0.488 N·m/kg for the ankle plantarflexion/dorsiflexion actuator (Figure 4.12). A larger standard deviation across subjects may correspond to greater difficulty in developing a single device that would accommodate different subjects and walking styles [29].

The zero-crossings in the torque profiles indicate where the actuator torques switch between flexion and extension (or between abduction and adduction). It is important for the zero-crossings to be correct: if a device mistimes a zero-crossing, it would be generating a flexion torque when an extension torque would be beneficial, for example. Thus, the differences in the standard deviation in the horizontal direction (specifically, where the curve crosses zero) are also important to note. In this regard, the hip abduction/adduction actuator may be most promising since it appears that the device could be designed to provide only an abduction torque without loss of effectiveness (thereby avoiding the issue altogether).

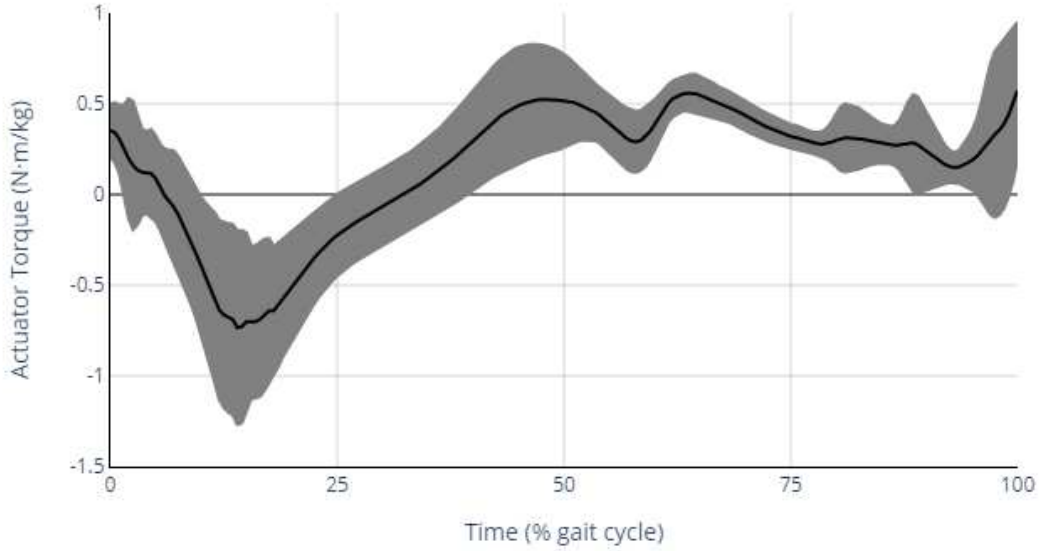

Figure 4.9. Torque generated by the ideal hip flexion/extension actuator. Mean (solid line) and standard deviation (shaded region) are shown for 10 elderly subjects (one leg from each subject). Flexion is positive.

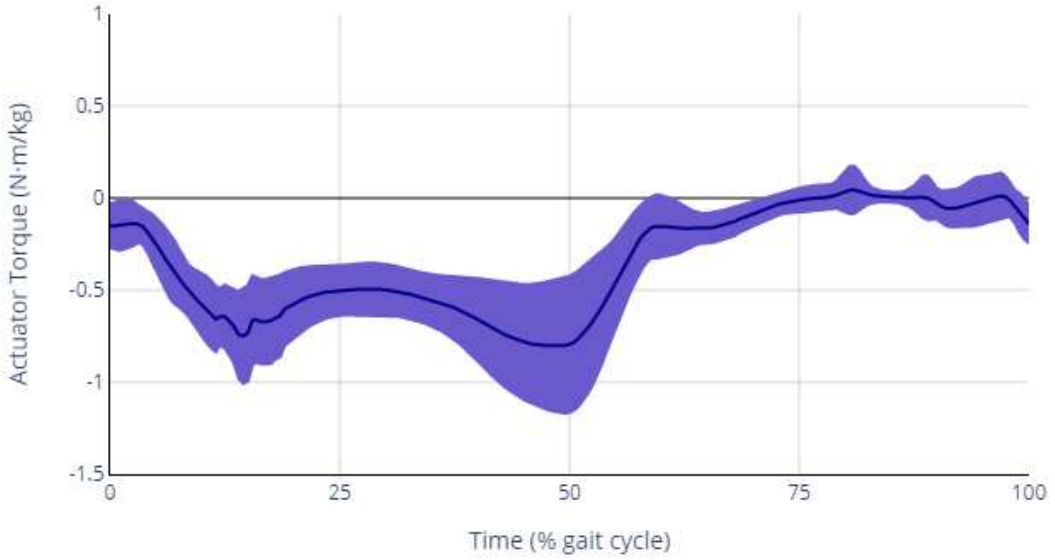

Figure 4.10. Torque generated by the ideal hip abduction/adduction actuator. Mean (solid line) and standard deviation (shaded region) are shown for 10 elderly subjects (one leg from each subject). Adduction is positive.

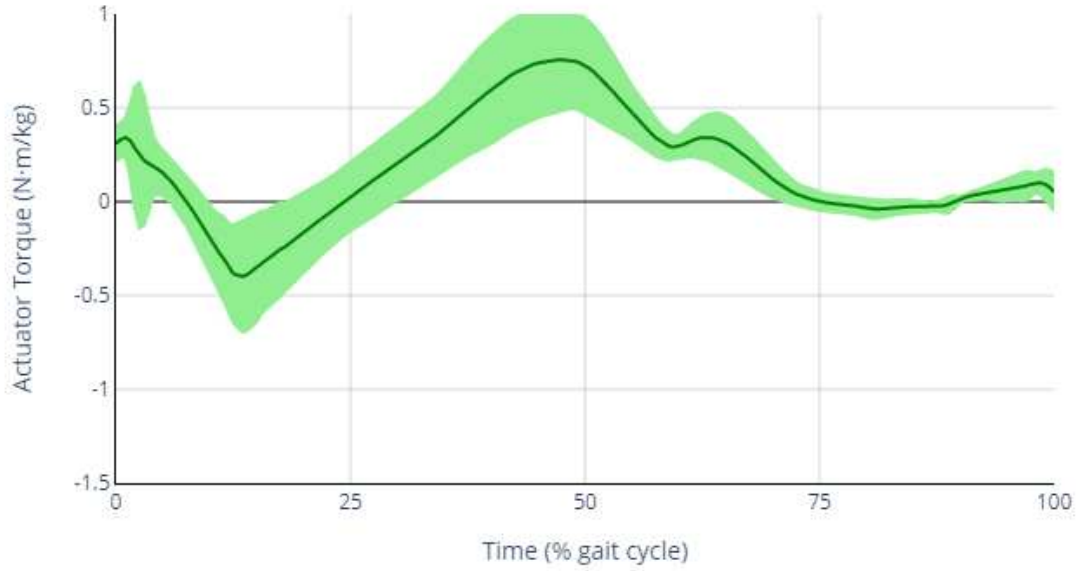

Figure 4.11. Torque generated by the ideal knee flexion/extension actuator. Mean (solid line) and standard deviation (shaded region) are shown for 10 elderly subjects (one leg from each subject). Flexion is positive.

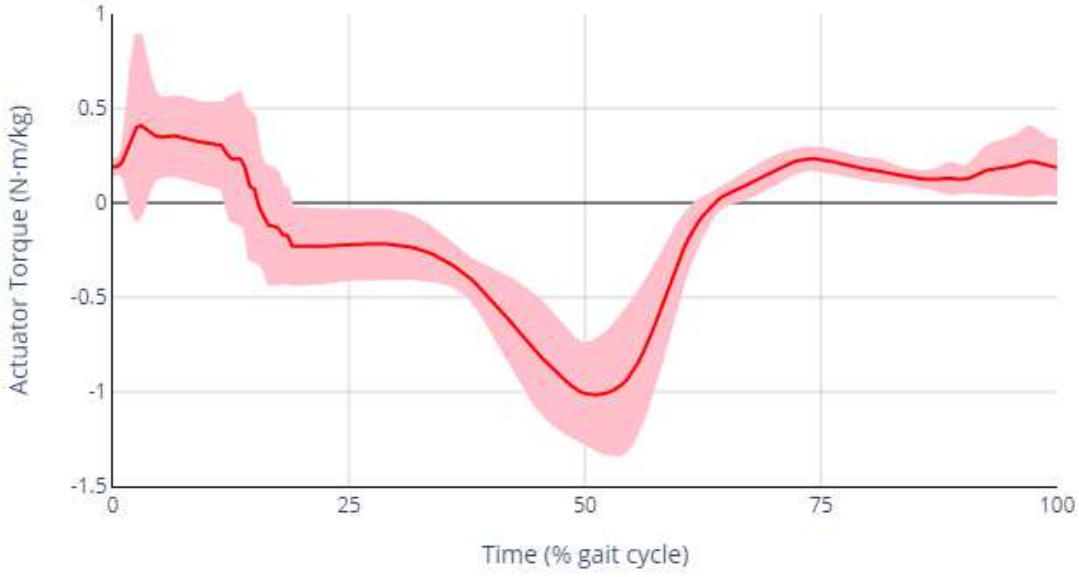

Figure 4.12. Torque generated by the ideal ankle plantarflexion/dorsiflexion actuator. Mean (solid line) and standard deviation (shaded region) are shown for 10 elderly subjects (one leg from each subject). Dorsiflexion is positive.

4.5. SIMULATIONS OF TORQUE-LIMITED DEVICES

An additional 120 CMC simulations were generated to explore the degradation in performance when torque limits were imposed on the simulated assistive devices. We simulated hip flexion/extension, hip abduction/adduction, knee flexion/extension and ankle plantarflexion/dorsiflexion assistance when limited to 25%, 50% and 75% of the maximum torque magnitude from the ideal assistance simulations. The torque limits were computed for each subject, assistance condition, and leg by reading the torque generated by the corresponding ideal actuator and limiting the maximum torque to 25%, 50% or 75% of the maximum absolute value. As an example, Figure 4.13 shows the torque generated by the ideal ankle plantarflexion/dorsiflexion actuator for the right leg of one subject and the torque applied by an actuator whose torque is limited to 50% of the maximum absolute value.

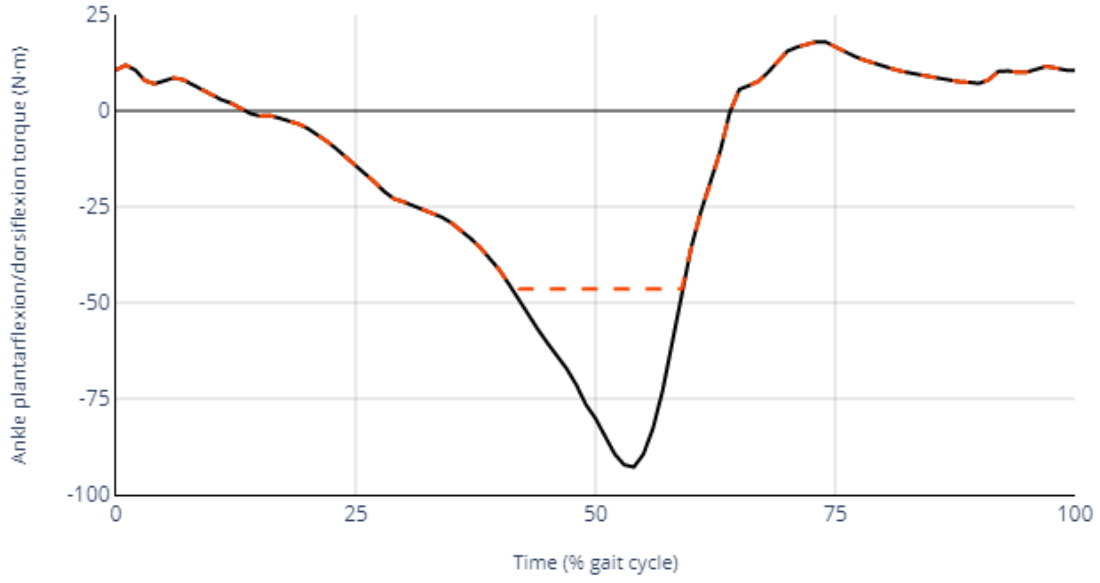

Figure 4.13. Example of the torque generated by an ideal actuator (black) and the torque applied by the corresponding torque-limited actuator (orange) over the gait cycle for one leg of one subject.

A 20% reduction in metabolic cost was observed when torque was limited to 50% in the hip flexion/extension actuators compared to a 24% reduction when using the ideal hip flexion/extension actuators (Figure 4.14). A 12% reduction in metabolic cost was observed when assisting with the 50%-torque-limited hip abduction/adduction actuators as compared to a 15% savings with the ideal hip abduction/adduction actuators. The 50%-torque-limited knee flexion/extension actuators resulted in a reduction of 17% compared to 20% when assisted by the ideal knee flexion/extension actuators. These results are particularly promising for assisting elderly people, assuming that it would be especially challenging to apply large torques to the limbs in this population. Note that, for the simulated ankle plantarflexion/dorsiflexion devices, only about half the savings were obtained when the maximum device torque was limited to 75% of the maximum ideal torque, suggesting that an ankle plantarflexion/dorsiflexion device may be a particularly poor choice for assisting elderly individuals.

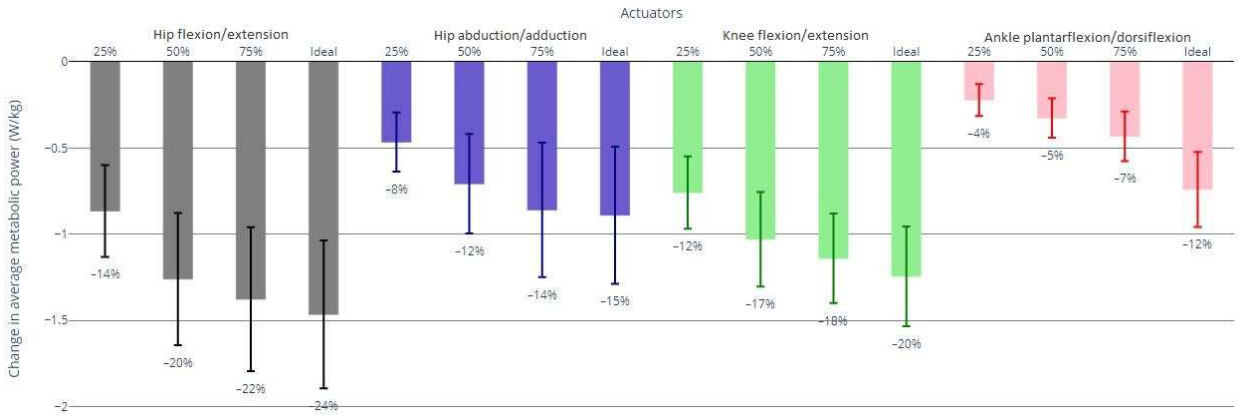

Figure 4.14. Metabolic savings with torque-limited assistance. Maximum actuator torque was limited to 25%, 50%, or 75% of the peak absolute value of the torque generated by the corresponding ideal actuator.

Table 4.6 shows the results of ANOVA and paired t-tests to determine whether the apparent differences shown in Figure 4.14 are in fact statistically significant. An ANOVA test showed significant differences in hip flexion/extension, hip abduction/adduction, and knee

flexion/extension devices. Of all the paired t-tests, only four comparisons were not significant (highlighted in Table 4.6, thus rejecting the null hypothesis. For the hip flexion/extension and knee flexion/extension devices, we found no statistically significant difference between the 75%-torque-limited and ideal devices (Tables 4.6(a) and (c)), suggesting that applying only up to 75% of the maximum torque magnitude from the ideal device may provide most of the metabolic benefit. For the hip abduction/adduction devices, there was no significant difference between the 50%-torque-limited and 75%-torque-limited devices, nor between the 75%-torque-limited and ideal devices (Table 4.6(b)). Finally, we found that there is a statistically significant difference between each test for the ankle plantarflexion/dorsiflexion devices (Table 4.6(d)), even though the standard deviations shown in Figure 4.14 are relatively large.

(a) Hip flexion/extension devices ANOVA: $p = 6.0 \times 10^{-3}$				
	25%	**50%**	**75%**	**Ideal**
25%	—			
50%	4.1×10^{-6}	—		
75%	5.5×10^{-6}	7.0×10^{-4}	—	
Ideal	1.6×10^{-6}	5.5×10^{-5}	1.1×10^{-2}	—

(b) Hip abduction/adduction devices ANOVA: $p = 2.4 \times 10^{-2}$				
	25%	**50%**	**75%**	**Ideal**
25%	—			
50%	3.4×10^{-4}	—		
75%	5.4×10^{-4}	1.3×10^{-3}	—	
Ideal	3.9×10^{-4}	6.0×10^{-4}	2.5×10^{-3}	—

(c) Knee flexion/extension devices ANOVA: $p = 1.3 \times 10^{-3}$				
	25%	**50%**	**75%**	**Ideal**
25%	—			
50%	1.1×10^{-4}	—		
75%	2.0×10^{-5}	1.7×10^{-4}	—	
Ideal	1.4×10^{-5}	2.1×10^{-4}	1.3×10^{-3}	—

(d) Ankle plantarflexion/dorsiflexion devices ANOVA: $p = 2.4 \times 10^{-8}$				
	25%	**50%**	**75%**	**Ideal**
25%	—			
50%	2.5×10^{-5}	—		
75%	3.5×10^{-5}	8.6×10^{-4}	—	
Ideal	9.5×10^{-6}	3.8×10^{-5}	2.5×10^{-4}	—

Table 4.6. Results of ANOVA and paired t-tests between torque-limited and ideal assistive devices.

CHAPTER 5: CONCLUSIONS

This chapter summarizes the contributions of this study, discuss the study limitations, and suggests directions for future work.

5.1. STUDY CONTRIBUTIONS

Walking assist exoskeletons (WAEs) offer a promising solution for restoring, enhancing, and maintaining mobility in elderly individuals. In this study, musculoskeletal models and simulations were used in OpenSim to analyze the effect of ideal and torque-limited assistive devices on healthy elderly gait. This work provides insight into the biological factors that may affect device performance and demonstrates the potential for simulations to complement experimental approaches to device design. This study provides suggestions for deciding which assistance strategies to pursue further in experimental studies. The torque profiles for each assistive device are reported in this study, which may be useful for device designers when selecting motors and batteries, and when determining the magnitude and timing of torques to apply. To date, most WAE research has focused on assisting the ankle, yet the simulations in this study suggest that assisting the hip or knee may lead to greater metabolic savings than assisting the ankle—and may offer advantages for the elderly population in particular. Assisting knee flexion/extension and hip abduction may be effective strategies to reduce metabolic cost, yet these strategies have not been explored in depth. The results of this study can be used to guide the future design and development of exoskeletons for the elderly population.

5.2. STUDY LIMITATIONS

Several limitations should be considered when interpreting the results of this study. This section discusses the limitations associated with data collection, model parameters, simulation and analysis.

5.2.1. DATA COLLECTION

One limitation is that the kinematic data used to generate the simulations were obtained from a public database. Some aberrations may have been encountered during data acquisition or post-processing stages that were considered inconsequential in the original study, but which may have affected the accuracy of our OpenSim simulations. This study does not account for any errors that may have occurred during the data acquisition process, such as marker placement errors, during the scaling process in OpenSim.

Furthermore, limited data were provided to customize the model for each subject. For example, the strength of the participants was not reported, which limited our ability to customize the muscle model parameters. To reflect muscular characteristics of the participants more accurately, muscle characteristics such as optimal fiber length and moment arms would need to be evaluated prior to conducting simulations. This study does not consider individual variations in muscle strength or characteristics between participants.

There is a wide range of walking speeds in our study, but it is unclear whether the participants were walking at subjectively fast or slow speeds. The simulated data were obtained when participants were instructed to walk at a comfortable pace. Because a comfortable speed is different for each subject, this resulted in each subject having different amounts of muscle activity in the simulations we generated. Information related to the fitness levels of these participants (e.g.,

muscular strength, flexibility, aerobic endurance, etc.) was not available. The availability of more data or more subjects with similar ages, BMI, and comfortable walking pace may provide results with better statistical power.

5.2.2. MODEL PARAMETERS

We assumed that all the muscles have same normalized force–length and force–velocity curves. This study does not account for individual differences in parameters that were not measured, such as optimal fiber length and tendon slack length.

As described in Chapter 3, we applied the same adjustments to the muscle parameters for all muscles and all models, as suggested by Thelen [48], which ignores the potential effects of age, sex, BMI, etc. Compared to young adults, elderly individuals tend to exhibit decreased muscle strength, prolonged twitch contractions, increased passive stiffness, and reduced rate of muscle force development. However, how these factors combine to contribute to slowing of the maximum contraction velocity of whole human muscle is difficult to measure and consequently not well documented [48]. Moreover, the parameter adjustments proposed by Thelen [48] were validated only for muscles crossing the ankle joint and have not been validated for other lower-extremity muscles. The muscle parameter adjustments made in the models were qualitatively consistent with observed age-related changes in muscle; however, the quantitative magnitudes of the adjustments are less definitive.

Another limitation of our study is that the modelled ideal assistive devices were massless and were able to produce arbitrary amounts of torque instantaneously. Adding mass to the leg increases energy expenditure [29, 62] and limiting the amount and rate of torque generation will reduce device effectiveness. However, reducing the amount of torque applied may not affect metabolic cost substantially (Figure 4.14).

5.2.3. SIMULATION AND ANALYSIS

An important limitation is that we assumed the kinematics and ground reaction forces (GRFs) would remain unchanged when subjects walked with assistance. In fact, an individual may change their kinematics when wearing an assistive device—potentially only temporarily as they learn to use the device but potentially in the long term as well. The ideal devices were simulated so one might expect experimental studies to see lower savings; however, the changes in kinematics or GRFs were not simulated, which may have the effect of increasing savings. Some studies suggest that joint kinematics may not change substantially when assisted [26, 57, 58] while other studies report relatively large changes in kinematics [59, 60]. Changes in kinematics do not necessarily cause substantial changes in metabolic cost [61], so this limitation of our study may not in fact affect our general conclusions.

We also note a specific weakness of the CMC algorithm: while substantial, the reductions in metabolic cost of uniarticular muscles spanning assisted joints should theoretically have been 100% since it would have been "free" for the actuator to generate these torques. The CMC Tool attempts to minimize the error between the internal forward simulations and the experimental kinematic data. However, the trajectory of the model diverges over time due to the accumulation of tracking errors; this is observed as drift toward the end of simulations. As described in Chapter 3, we assumed symmetry to analyze one full gait cycle which may not be perfectly symmetric. In fact, half of a gait cycle could be simulated to avoid the aforementioned issue with the CMC optimizer. Despite the fact that the globally optimal solution to the minimization problem was not always found by the optimizer in our simulations, the metabolic costs still tended to be low in the expected muscles. For example, the vasti and biceps femoris short head have low metabolic cost (0.222 W/kg and 0.044 W/kg, respectively) when assisting knee flexion/extension (see Figure 4.4).

Finally, we did not simulate muscle fatigue, which may affect muscle recruitment strategies. For example, the activity of the rectus femoris increased during stance when the ideal hip flexion/extension and knee flexion/extension actuators were added to the models (see Figures 4.5 and 4.7). However, the rectus femoris was lengthening while generating large forces and would, therefore, be susceptible to fatigue [63]. Furthermore, the rectus femoris is comprised of primarily fast-twitch muscle fibers [64], which are more prone to fatigue than slow-twitch fibers [65]. Nevertheless, it may be possible to design a device that has the same effect as increasing the activity of the rectus femoris in our simulations [29].

5.3. FUTURE WORK

This study suggests several experimental and computational research avenues to predict and gain insight into the energetic effects of assisted walking. The study demonstrates the potential for simulation to complement experimental approaches to design a device. Simulations were used to predict the energetic effects of ideal and torque-limited assistive devices during gait in elderly individuals. An obvious next step is to validate our predictions experimentally and to extend them to walking at different speeds. In the future, the simulated muscle activities could be compared to EMG data from experiments and/or previous studies. This would help to determine whether onset/offset timing in experiments and simulations are in good agreement.

Future work could also involve studying more personalized or more complicated devices. For example, many existing devices provide assistance to more than one joint. Experimental data from a larger sample size could be used to improve the robustness of the results and to explore the variety of elderly gait patterns more fully. We also ignored the mass of the device, which is known to affect device performance—particularly if the mass is located distally [29, 62]. Finally, our

approach could be extended to investigate other factors we did not consider in this study, such as muscle fatigue and the study of specific device designs.

A key limitation of this study was the assumption that the subject's kinematics would not change substantially when assistance was added, or that the kinematics would change initially and then return to normal. Although some experimental studies support this assumption, others do not. It would be valuable to explore device performance in simulation without making this assumption. However, allowing the kinematics to change would require an entirely different simulation strategy. One approach would be to use a controller to generate muscle excitations that are then used to drive a forward dynamic simulation. An optimizer would be used to find muscle excitations over time that produce a walking pattern. This simulation strategy has been effective in other studies [66] and would be useful to explore in the context of elderly gait as well.

REFERENCES

[1] P. Mahlknecht, S. Kiechl, B. R. Bloem, J. Willeit, C. Scherfler, A. Gasperi, G. Rungger, W. Poewe, K. Seppi, "Prevalence and burden of gait disorders in elderly men and women aged 60–97 years: A population-based study," PLOS ONE, vol. 8, no. 7, p. e69627, 2013, doi: 10.1371/journal.pone.0069627

[2] F. Prince, H. Corriveau, R. Hébert, and D. A. Winter, "Gait in the elderly," Gait Posture, vol. 5, no. 2, pp. 128–135, 1997, doi: 10.1016/S0966-6362(97)01118-1

[3] S. H. Lee, H. J. Lee, W. H. Chang, B. O. Choi, J. Lee, J. Kim, G. H. Ryu, Y. H. Kim, "Gait performance and foot pressure distribution during wearable robot-assisted gait in elderly adults," J. NeuroEngineering Rehabil., vol. 14, no. 1, p. 123, 2017, doi: 10.1186/s12984-017-0333-z

[4] S. Studenski, "Gait speed and survival in older adults," JAMA, vol. 305, no. 1, p. 50, 2011, doi: 10.1001/jama.2010.1923

[5] B. S. Rupal, S. Rafique, A. Singla, E. Singla, M. Isaksson, and G. S. Virk, "Lower-limb exoskeletons: Research trends and regulatory guidelines in medical and non-medical applications," Int. J. Adv. Robot. Syst., vol. 14, no. 6, p. 172988141774355, 2017, doi: 10.1177/1729881417743554

[6] C. L. Dembia, A. Silder, T. K. Uchida, J. L. Hicks, and S. L. Delp, "Simulating ideal assistive devices to reduce the metabolic cost of walking with heavy loads," PLOS ONE, vol. 12, no. 7, p. e0180320, 2017, doi: 10.1371/journal.pone.0180320

[7] A. Seth, J. L. Hicks, T. K. Uchida, A. Habib, C. L. Dembia, J. J. Dunne, C. F. Ong, M. S. DeMers, A. Rajagopal, M. Millard, S. R. Hamner, E. M. Arnold, J. R. Yong, S. K. Lakshmikanth, M. A. Sherman, J. P. Ku, S. L. Delp, "OpenSim: Simulating musculoskeletal dynamics and neuromuscular control to study human and animal movement," PLOS Comput. Biol., vol. 14, no. 7, p. e1006223, 2018, doi: 10.1371/journal.pcbi.1006223

[8] T. K. Uchida, S. L. Delp, Biomechanics of Movement: The Science of Sports, Robotics, and Rehabilitation. Cambridge, Massachusetts: The MIT Press, 2020, ISBN: 9780262044202

[9] W. Pirker and R. Katzenschlager, "Gait disorders in adults and the elderly: A clinical guide," Wien. Klin. Wochenschr., vol. 129, no. 3–4, pp. 81–95, 2017, doi: 10.1007/s00508-016-1096-4

[10] D. A. Winter, Biomechanics and Motor Control of Human Movement, 4th ed. Hoboken, N.J.: Wiley, 2009, ISBN: 978-0-470-39818-0

[11] C. A. McGibbon, “Toward a better understanding of gait changes with age and disablement: Neuromuscular adaptation,” Exerc. Sport Sci. Rev., vol. 31, no. 2, pp. 102–108, 2003, doi: 10.1097/00003677-200304000-00009

[12] J. O. JudgeRoy, B. Davis, and S. Ounpuu, “Step length reductions in advanced age: The role of ankle and hip kinetics,” J. Gerontol. A. Biol. Sci. Med. Sci., vol. 51A, no. 6, pp. M303–M312, 1996, doi: 10.1093/gerona/51A.6.M303

[13] W. S. Kim and E. Y. Kim, “Comparing self-selected speed walking of the elderly with self-selected slow, moderate, and fast speed walking of young adults,” Ann. Rehabil. Med., vol. 38, no. 1, p. 101, 2014, doi: 10.5535/arm.2014.38.1.101

[14] D. A. Winter, The Biomechanics and Motor Control of Human Gait: Normal, Elderly and Pathological, 2nd ed. Waterloo, Ont., 1991, ISBN 0-88898-105-8

[15] L. Larsson, G. Grimby, and J. Karlsson, “Muscle strength and speed of movement in relation to age and muscle morphology,” J. Appl. Physiol., 1979, doi: 10.1152/jappl.1979.46.3.451

[16] S. M. Bradley and C. R. Hernandez, “Geriatric assistive devices,” American Family Physician, vol. 84, no. 4, p. 7, 2011, PMID: 21842786

[17] H. J. Lee, S. Lee, W. H. Chang, K. Seo, Y. Shim, B. O. Choi, G. H. Ryu, Y. H. Kim, “A wearable hip assist robot can improve gait function and cardiopulmonary metabolic efficiency in elderly adults,” IEEE Trans. Neural Syst. Rehabil. Eng., vol. 25, no. 9, pp. 1549–1557, 2017, doi: 10.1109/TNSRE.2017.2664801

[18] Q. Wu, X. Wang, F. Du, and X. Zhang, “Design and control of a powered hip exoskeleton for walking assistance,” Int. J. Adv. Robot. Syst., vol. 12, no. 3, p. 18, 2015, doi: 10.5772/59757

[19] “Walking Assist,” Exoskeleton Report, 2016. https://exoskeletonreport.com/product/honda-walking-assist (accessed Oct. 6, 2020).

[20] C. Buesing, G. Fisch, M. O’Donnell, I. Shahidi, L. Thomas, C. K. Mummidisetty, K. J. Williams, H. Takahashi, W. Z. Rymer, A. Jayaraman, “Effects of a wearable exoskeleton stride management assist system (SMA®) on spatiotemporal gait characteristics in individuals after stroke: A randomized controlled trial,” J. NeuroEngineering Rehabil., vol. 12, no. 1, p. 69, 2015, doi: 10.1186/s12984-015-0062-0

[21] G. S. Sawicki, O. N. Beck, I. Kang, and A. J. Young, “The exoskeleton expansion: Improving walking and running economy,” J. NeuroEngineering Rehabil., vol. 17, no. 1, p. 25, 2020, doi: 10.1186/s12984-020-00663-9

[22] A. J. van den Bogert, “Exotendons for assistance of human locomotion,” Biomed. Eng. OnLine, vol. 2, no. 1, p. 17, 2003, doi: 10.1186/1475-925X-2-17

[23] W. van Dijk and H. Van der Kooij, “XPED2: A passive exoskeleton with artificial tendons,” IEEE Robot. Autom. Mag., vol. 21, no. 4, pp. 56–61, 2014, doi: 10.1109/MRA.2014.2360309

[24] S. Krut, M. Benoit, E. Dombre, and F. Pierrot, “MoonWalker, a lower limb exoskeleton able to sustain bodyweight using a passive force balancer,” p. 7, 2010, doi: 10.1109/ROBOT.2010.5509961

[25] Z. Lovrenovic and M. Doumit, “Development and testing of a passive walking assist exoskeleton,” Biocybern. Biomed. Eng., vol. 39, no. 4, pp. 992–1004, 2019, doi: 10.1016/j.bbe.2019.01.002

[26] S. H. Collins, M. B. Wiggin, and G. S. Sawicki, “Reducing the energy cost of human walking using an unpowered exoskeleton,” Nature, vol. 522, no. 7555, p. 7555, 2015, doi: 10.1038/nature14288

[27] M. Ishikawa, P. V. Komi, M. J. Grey, V. Lepola, and G. P. Bruggemann, “Muscle-tendon interaction and elastic energy usage in human walking,” J. Appl. Physiol., vol. 99, no. 2, pp. 603–608, 2005, doi: 10.1152/japplphysiol.00189.2005

[28] T. K. Uchida, J. L. Hicks, C. L. Dembia, and S. L. Delp, “Stretching your energetic budget: How tendon compliance affects the metabolic cost of running,” PLOS ONE, vol. 11, no. 3, p. e0150378, 2016, doi: 10.1371/journal.pone.0150378

[29] T. K. Uchida, A. Seth, S. Pouya, C. L. Dembia, J. L. Hicks, and S. L. Delp, “Simulating ideal assistive devices to reduce the metabolic cost of running,” PLOS ONE, vol. 11, no. 9, p. e0163417, 2016, doi: 10.1371/journal.pone.0163417

[30] D. P. Ferris, G. S. Sawicki, and M. A. Daley, “A physiologist’s perspective on robotic exoskeletons for human locomotion,” Int. J. Humanoid Robot., vol. 4, no. 3, pp. 507–528, 2007, doi: 10.1142/S0219843607001138

[31] S. L. Delp, F. C. Anderson, A. S. Arnold, P. Loan, A. Habib; C. T. John, E. Guendelman, D. G. Thelen, “OpenSim: Open-Source software to create and analyze dynamic simulations of movement,” IEEE Trans. Biomed. Eng., vol. 54, no. 11, pp. 1940–1950, 2007, doi: 10.1109/TBME.2007.901024

[32] “Visual3D Overview - Visual3D Wiki Documentation.” https://www.c-motion.com/v3dwiki/index.php/Visual3D_Overview (accessed Oct. 23, 2020).

[33] J. B. Langholz, G. Westman, and M. Karlsteen, “Musculoskeletal modelling in sports - Evaluation of different software tools with focus on swimming,” Procedia Eng., vol. 147, pp. 281–287, 2016, doi: 10.1016/j.proeng.2016.06.278

[34] “Biomechanics of Bodies (BoB),” bob-biomechanics.com. https://www.bob-biomechanics.com (accessed Oct. 23, 2020).

[35] K. R. S. Holzbaur, W. M. Murray, and S. L. Delp, "A model of the upper extremity for simulating musculoskeletal surgery and analyzing neuromuscular control," Ann. Biomed. Eng., vol. 33, no. 6, pp. 829–840, 2005, doi: 10.1007/s10439-005-3320-7

[36] S. L. Delp, J. P. Loan, M. G. Hoy, F. E. Zajac, E. L. Topp, and J. M. Rosen, "An interactive graphics-based model of the lower extremity to study orthopaedic surgical procedures," IEEE Trans. Biomed. Eng., vol. 37, no. 8, pp. 757–767, 1990, doi: 10.1109/10.102791

[37] A. Rajagopal, C. L. Dembia, M. S. DeMers, D. D. Delp, J. L. Hicks, and S. L. Delp, "Full-body musculoskeletal model for muscle-driven simulation of human gait," IEEE Trans. Biomed. Eng., vol. 63, no. 10, pp. 2068–2079, 2016, doi: 10.1109/TBME.2016.2586891

[38] A. Seth, M. Sherman, J. A. Reinbolt, and S. L. Delp, "OpenSim: A musculoskeletal modeling and simulation framework for in silico investigations and exchange," Procedia IUTAM, vol. 2, pp. 212–232, 2011, doi: 10.1016/j.piutam.2011.04.021

[39] G. Valente, G. Crimi, N. Vanella, E. Schileo, and F. Taddei, "nms Builder: Freeware to create subject-specific musculoskeletal models for OpenSim," Comput. Methods Programs Biomed., vol. 152, pp. 85–92, 2017, doi: 10.1016/j.cmpb.2017.09.012

[40] S. R. Hamner, A. Seth, and S. L. Delp, "Muscle contributions to propulsion and support during running," J. Biomech., vol. 43, no. 14, pp. 2709–2716, 2010, doi: 10.1016/j.jbiomech.2010.06.025

[41] J. L. Hicks, T. K. Uchida, A. Seth, A. Rajagopal, and S. L. Delp, "Is my model good enough? Best practices for verification and validation of musculoskeletal models and simulations of movement," J. Biomech. Eng., vol. 137, no. 2, p. 020905, 2015, doi: 10.1115/1.4029304

[42] C. A. Fukuchi, R. K. Fukuchi, and M. Duarte, "A public dataset of overground and treadmill walking kinematics and kinetics in healthy individuals," PeerJ, vol. 6, p. e4640, 2018, doi: 10.7717/peerj.4640

[43] "Preparing Your Data - OpenSim Documentation - Global Site." https://simtk-confluence.stanford.edu/display/OpenSim/Preparing+Your+Data (accessed Oct. 4, 2020).

[44] "Scaling - OpenSim Documentation - Global Site." https://simtk-confluence.stanford.edu/display/OpenSim/Scaling (accessed Oct. 4, 2020).

[45] F. E. Zajac, "Muscle and tendon: Properties, models, scaling, and application to biomechanics and motor control," Crit. Rev. Biomed. Eng., vol. 17, no. 4, pp. 359–411, 1989, PMID: 2676342

[46] "How to Use the Scale Tool - OpenSim Documentation - Global Site." https://simtk-confluence.stanford.edu/display/OpenSim/How+to+Use+the+Scale+Tool (accessed Oct. 4, 2020).

[47] "How to Use the Scale Tool - OpenSim Documentation - Global Site." https://simtk-confluence.stanford.edu/display/OpenSim/How+to+Use+the+Scale+Tool#HowtoUsetheScaleTool-UsingMeasurement-BasedScaling (accessed Oct. 4, 2020).

[48] D. G. Thelen, "Adjustment of muscle mechanics model parameters to simulate dynamic contractions in older adults," J. Biomech. Eng., vol. 125, no. 1, pp. 70–77, 2003, doi: 10.1115/1.1531112

[49] D. G. Thelen and F. C. Anderson, "Using computed muscle control to generate forward dynamic simulations of human walking from experimental data," J. Biomech., vol. 39, no. 6, pp. 1107–1115, 2006, doi: 10.1016/j.jbiomech.2005.02.010

[50] "How RRA Works - OpenSim Documentation - Global Site." https://simtk-confluence.stanford.edu:8443/display/OpenSim/How+RRA+Works (accessed Sep. 23, 2020).

[51] B. R. Umberger, "Stance and swing phase costs in human walking," J. R. Soc. Interface, vol. 7, no. 50, pp. 1329–1340, 2010, doi: 10.1098/rsif.2010.0084

[52] B. R. Umberger, K. G. M. Gerritsen, and P. E. Martin, "A model of human muscle energy expenditure," Comput. Methods Biomech. Biomed. Engin., vol. 6, no. 2, pp. 99–111, 2003, doi: 10.1080/1025584031000091678

[53] J. K. Rathkey and C. M. Wall-Scheffler, "People choose to run at their optimal speed: Rathkey and Wall-scheffler," Am. J. Phys. Anthropol., vol. 163, no. 1, pp. 85–93, 2017, doi: 10.1002/ajpa.23187

[54] K. Seo, J. Lee, Y. Lee, T. Ha, and Y. Shim, "Fully autonomous hip exoskeleton saves metabolic cost of walking," in 2016 IEEE International Conference on Robotics and Automation (ICRA), 2016, pp. 4628–4635, doi: 10.1109/ICRA.2016.7487663

[55] Y. Ding, M. Kim, S. Kuindersma, and C. J. Walsh, "Human-in-the-loop optimization of hip assistance with a soft exosuit during walking," Sci. Robot., vol. 3, no. 15, p. eaar5438, 2018, doi: 10.1126/scirobotics.aar5438

[56] B. Lim, J. Lee, J. Jang, K. Kim, Y. J. Park, K. Seo, Y. Shim, "Delayed output feedback control for gait assistance with a robotic hip exoskeleton," IEEE Trans. Robot., vol. 35, no. 4, pp. 1055–1062, 2019, doi: 10.1109/TRO.2019.2913318

[57] P. C. Kao, C. L. Lewis, and D. P. Ferris, "Invariant ankle moment patterns when walking with and without a robotic ankle exoskeleton," J. Biomech., vol. 43, no. 2, pp. 203–209, 2010, doi: 10.1016/j.jbiomech.2009.09.030

[58] C. L. Lewis and D. P. Ferris, "Invariant hip moment pattern while walking with a robotic hip exoskeleton," J. Biomech., vol. 44, no. 5, pp. 789–793, 2011, doi: 10.1016/j.jbiomech.2011.01.030

[59] T. Lenzi, M. C. Carrozza, and S. K. Agrawal, “Powered hip exoskeletons can reduce the user’s hip and ankle muscle activations during walking,” IEEE Trans. Neural Syst. Rehabil. Eng., vol. 21, no. 6, pp. 938–948, 2013, doi: 10.1109/TNSRE.2013.2248749

[60] S. Galle, P. Malcolm, W. Derave, and D. De Clercq, “Adaptation to walking with an exoskeleton that assists ankle extension,” Gait Posture, vol. 38, no. 3, pp. 495–499, 2013, doi: 10.1016/j.gaitpost.2013.01.029

[61] M. T. Vanderpool, S. H. Collins, and A. D. Kuo, “Ankle fixation need not increase the energetic cost of human walking,” Gait Posture, vol. 28, no. 3, pp. 427–433, 2008, doi: 10.1016/j.gaitpost.2008.01.016

[62] R. C. Browning, J. R. Modica, R. Kram, and A. Goswami, “The effects of adding mass to the legs on the energetics and biomechanics of walking,” Med. Sci. Sports Exerc., vol. 39, no. 3, pp. 515–525, 2007, doi: 10.1249/mss.0b013e31802b3562

[63] D. J. Newham, K. R. Mills, B. M. Quigley, and R. H. T. Edwards, “Pain and fatigue after concentric and eccentric muscle contractions,” Clin. Sci., vol. 64, no. 1, pp. 55–62, 1983, doi: 10.1042/cs0640055

[64] W. E. Garrett, J. C. Califf, and F. H. Bassett, “Histochemical correlates of hamstring injuries,” Am. J. Sports Med., vol. 12, no. 2, pp. 98–103, 1984, doi: 10.1177/036354658401200202

[65] R. H. Fitts, “Cellular mechanisms of muscle fatigue,” Physiol. Rev., vol. 74, no. 1, pp. 49–94, 1994, doi: 10.1152/physrev.1994.74.1.49

[66] T. W. Dorn, J. M. Wang, J. L. Hicks, and S. L. Delp, “Predictive simulation generates human adaptations during loaded and inclined walking,” PLOS ONE, vol. 10, no. 4, p. e0121407, 2015, doi: 10.1371/journal.pone.0121407

[67] M. Millard, T. Uchida, A. Seth, and S. L. Delp, "Flexing computational muscle: modeling and simulation of musculotendon dynamics," J. Biomech. Eng., vol. 135, no. 2, p. 021005, 2013, doi: 10.1115/1.4023390

[68] Dahiru T. "P - value, a true test of statistical significance? A cautionary note," Ann Ib Postgrad Med. vol. 6, pp. 21-26, 2008, doi: 10.4314/aipm.v6i1.64038

[69] D. Lakens, “Calculating and reporting effect sizes to facilitate cumulative science: a practical primer for t-tests and ANOVAs,” Frontiers in Psychology, vol. 4, p. 863, 2013, doi: 10.3389/fpsyg.2013.00863

APPENDIX A: VERIFICATION OF RESULTS

This section provides additional information on the generation and verification of our simulations. Table A-1 shows the marker error output from the OpenSim Scale Tool for all models. Table A-2 shows the maker weights used in the IK Tool. Figure A-1 shows an example of the mass adjustments recommended by the RRA Tool.

Participant Identification Number	Total Squared Error	RMS Error (cm)	Maximum Marker Error (cm)
S29	0.064	0.481	0.834
S31	0.185	0.813	1.467
S32	0.127	0.675	1.242
S33	0.218	0.883	1.628
S34	0.039	0.377	0.692
S36	0.252	0.950	2.609
S37	0.081	0.539	0.772
S39	0.226	0.899	2.224
S40	0.099	0.595	1.204
S42	0.083	0.546	0.984

Table A-1. RMS marker error and the maximum marker error for 10 subjects.

Marker	Marker Weight
R.ASIS	10
L.ASIS	10
V.Sacral	10
R.Thigh.Upper	1
R.Thigh.Front	1
R.Thigh.Rear	1
R.Shank.Upper	1
R.Shank.Front	1
R.Shank.Rear	1
R.Heel	10
R.Midfoot.Sup	1
R.Midfoot.Lat	1
R.Toe.Lat	1
R.Toe.Med	1
R.Toe.Tip	10
L.Thigh.Upper	1
L.Thigh.Front	1
L.Thigh.Rear	1
L.Shank.Upper	1
L.Shank.Front	1
L.Shank.Rear	1
L.Heel	10
L.Midfoot.Sup	1
L.Midfoot.Lat	1
L.Toe.Lat	1
L.Toe.Med	1
L.Toe.Tip	10

Table A-2. Marker weights used to solve the weighted least-squares problem in the Inverse Kinematics Tool.

```
************************************************************
*      Summary of Mass Adjustments to Reduce Residuals     *
************************************************************
* Body adjusted: pelvis
* Mass Center (COM) adjustment: dx =-0.1, dz =-0.0280844
* New COM location: ~[0.0244317,0,0.0280844]
************************************************************
* Recommended mass adjustments:
*  Total mass change: -0.725675
*  pelvis: orig mass = 9.37747, new mass = 9.26376
*  femur_r: orig mass = 7.40626, new mass = 7.31646
*  tibia_r: orig mass = 2.95211, new mass = 2.91631
*  talus_r: orig mass = 0.0796252, new mass = 0.0786598
*  calcn_r: orig mass = 0.995316, new mass = 0.983248
*  toes_r: orig mass = 0.172468, new mass = 0.170377
*  femur_l: orig mass = 7.40626, new mass = 7.31646
*  tibia_l: orig mass = 2.95211, new mass = 2.91631
*  talus_l: orig mass = 0.0796252, new mass = 0.0786598
*  calcn_l: orig mass = 0.995316, new mass = 0.983248
*  toes_l: orig mass = 0.172468, new mass = 0.170377
*  torso: orig mass = 27.261, new mass = 26.9304
************************************************************
* Note: Edit the model to make recommended adjustments to  *
*       mass properties.                                   *
************************************************************
```

Figure A-1. Example of mass adjustments recommended by the RRA Tool.

The RRA and CMC simulation results were evaluated based on threshold values reported in the literature [41]. Table A-3 shows the maximum and average RMS residual forces and moments across 10 subjects for the RRA simulations; Table A-4 shows the same quantities for the CMC simulations of unassisted walking.

	F_x (N)	F_y (N)	F_z (N)	M_x (N·m)	M_y (N·m)	M_z (N·m)
Maximum	8.71	18.21	10.23	45.20	22.30	38.78
RMS	5.51	10.71	7.15	29.05	12.40	28.88

Table A-3. Maximum and average RMS residual forces and moments for RRA simulations of 10 subjects.

	F_x (N)	F_y (N)	F_z (N)	M_x (N·m)	M_y (N·m)	M_z (N·m)
Maximum	9.81	24.48	10.22	47.11	23.08	45.01
RMS	7.83	9.45	8.15	29.29	12.10	29.06

Table A-4. Maximum and average RMS residual forces and moments for CMC simulations of 10 subjects.

EFFECT SIZES

Statistical effect sizes were calculated to measure the sizes of differences between group means. Cohen's d formula [69] was used to calculate this effect size:

$$d = \frac{M_1 - M_2}{SD}$$

where M_1 and M_2 are the group means and SD is the standard deviation. An effect size of $d \leq 0.2$ is considered to be "small," 0.5 represents a "medium" effect size, and $d \geq 0.8$ represents a "large" effect size. In other words, if the difference between two group means is less than 0.2 standard deviations, the difference is not considered to be statistically significant. Tables A-5 and A-6 show, respectively, the effect sizes for comparisons between the four ideal assistive devices (see Figure 4.2) and between the ideal and torque-limited devices (see Figure 4.14).

GROUPS	EFFECT SIZE
Hip flexion/extension vs. Hip abduction/adduction	1.391
Hip flexion/extension vs. Knee flexion/extension	0.604
Hip flexion/extension vs. Ankle plantarflexion/dorsiflexion	2.131
Hip abduction/adduction vs. Knee flexion/extension	1.018
Hip abduction/adduction vs. Ankle plantarflexion/dorsiflexion	0.466
Knee flexion/extension vs. Ankle plantarflexion/dorsiflexion	1.966

Table A-5. Effect sizes for comparisons between four ideal assistive devices.

Device	25% vs. 50%	25% vs. 75%	25% vs. Ideal	50% vs. 75%	50% vs. Ideal	75% vs. Ideal
Hip flexion/extension	1.196	1.462	1.680	0.291	0.504	0.208
Hip abduction/adduction	1.017	1.304	1.383	0.441	0.524	0.078
Knee flexion/extension	1.108	1.615	1.921	0.414	0.761	0.378
Ankle plantarflexion/dorsiflexion	1.001	1.738	3.095	0.817	2.380	1.667

Table A-6. Effect sizes for comparisons between ideal and torque-limited devices.

APPENDIX B: ACTIVATIONS OF LOWER-EXTREMITY MUSCLES

This section presents the activations of all lower-extremity muscles for the leading leg (stepped on the force plate first; Figure B-1) and trailing leg (Figure B-2) for unassisted and assisted scenarios.

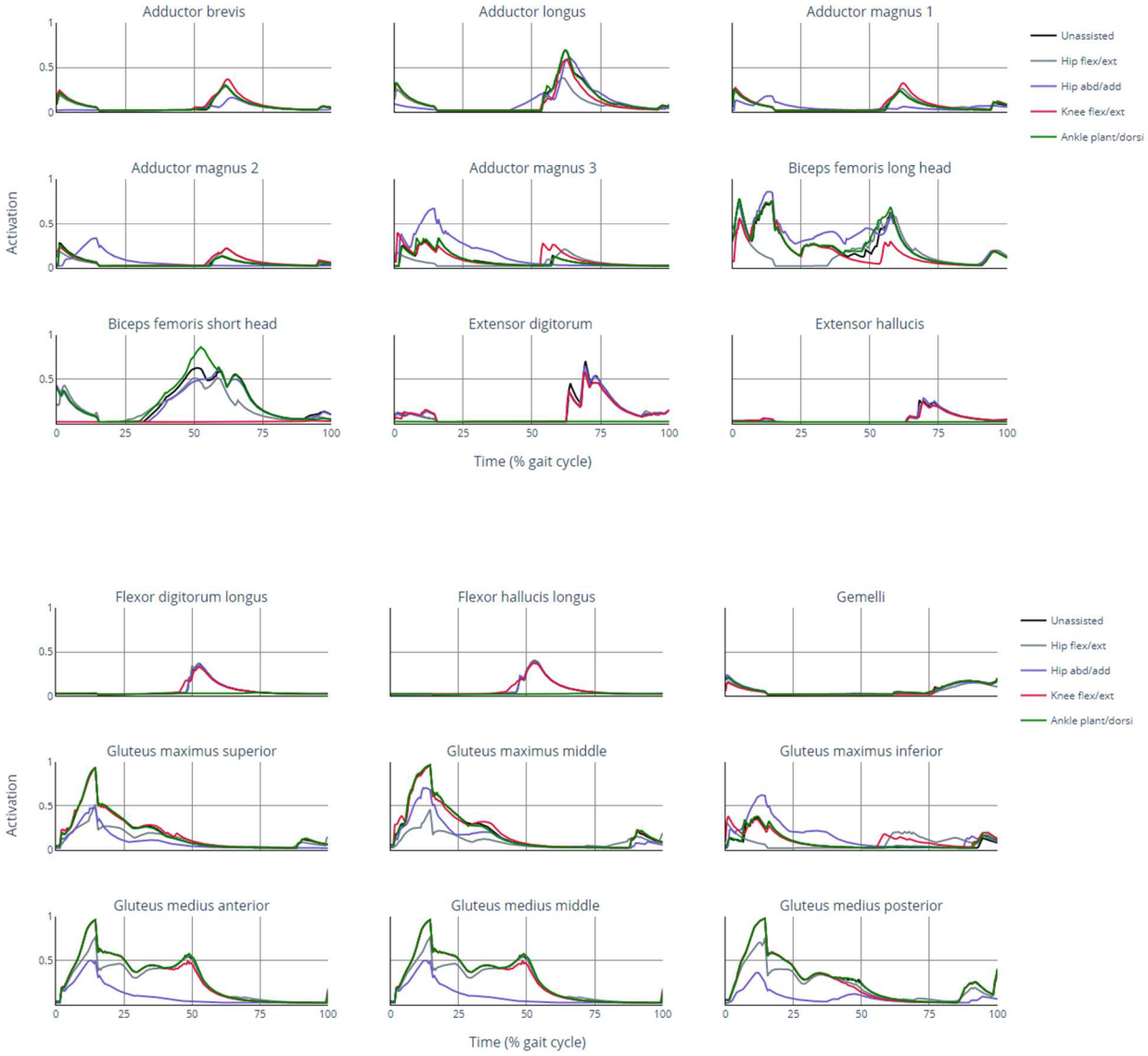

Figure B-1. Activations of all lower-extremity muscles for the leading leg when unassisted (black) and when assisting hip flexion/extension (grey), hip abduction/adduction (purple), knee flexion/extension (red), and ankle plantarflexion/dorsiflexion (green).

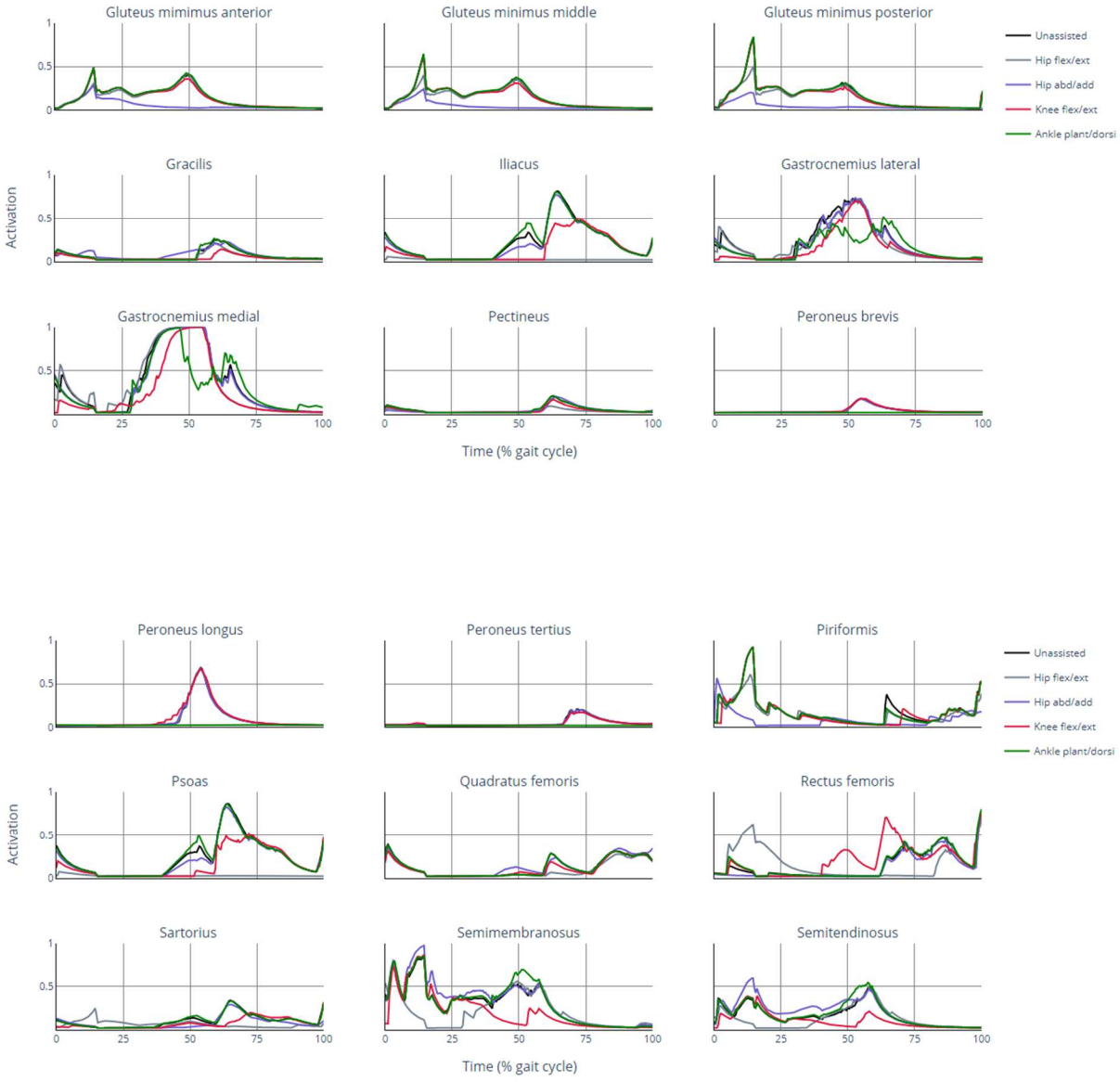

Figure B-1. Continued.

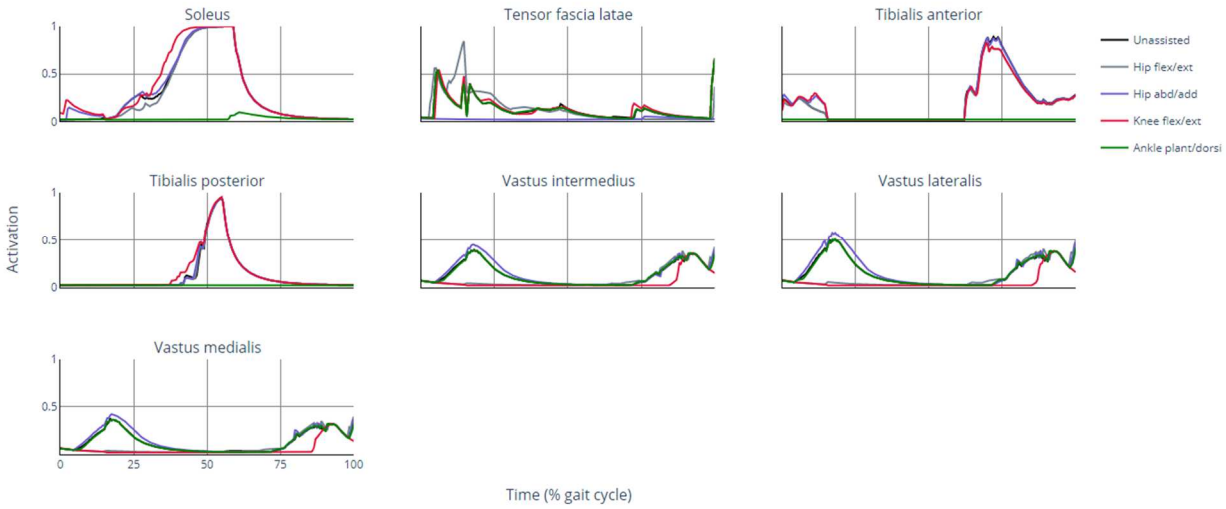

Figure B-1. Continued.

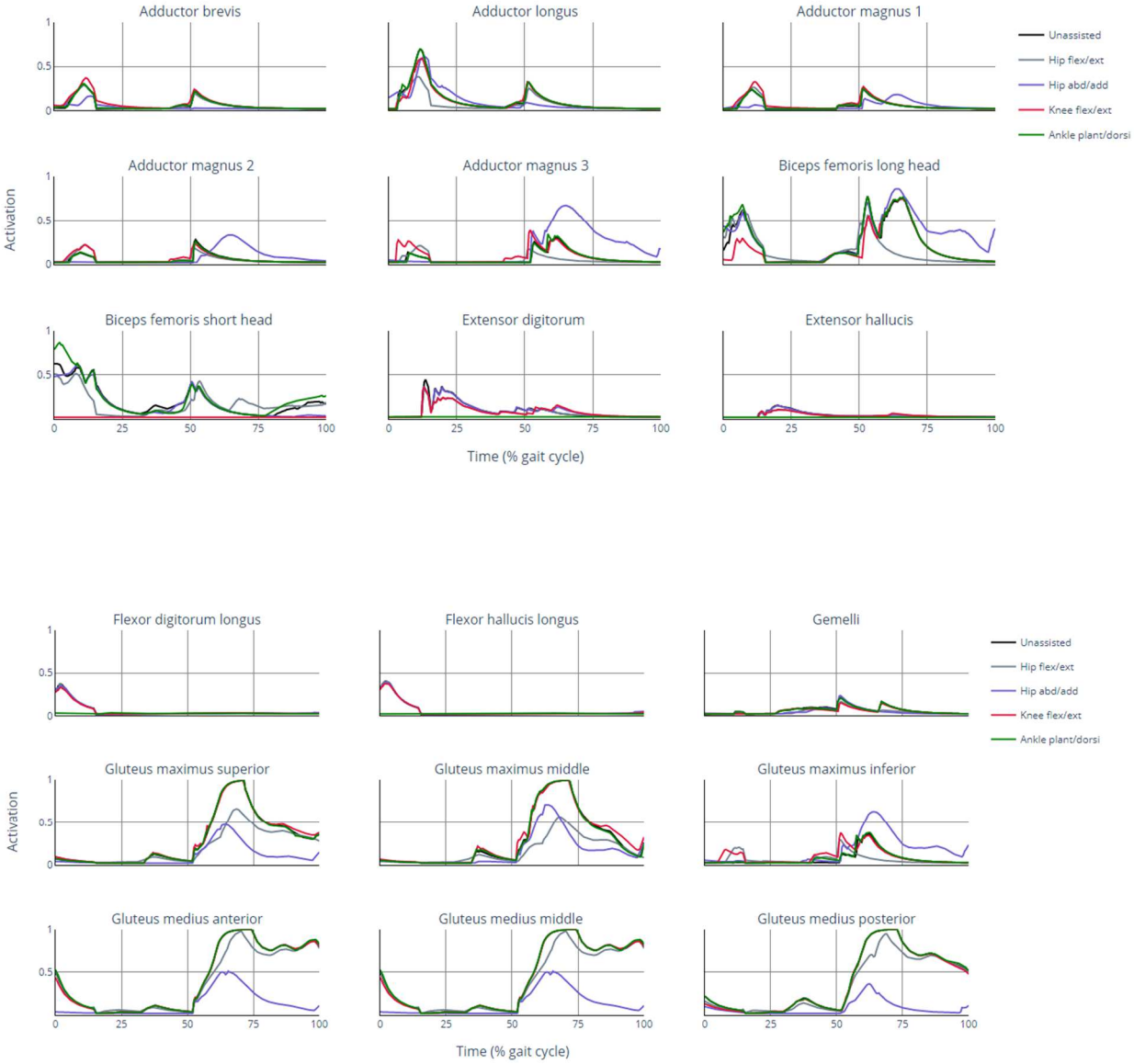

Figure B-2. Activations of all lower-extremity muscles for the trailing leg when unassisted (black) and when assisting hip flexion/extension (grey), hip abduction/adduction (purple), knee flexion/extension (red), and ankle plantarflexion/dorsiflexion (green).

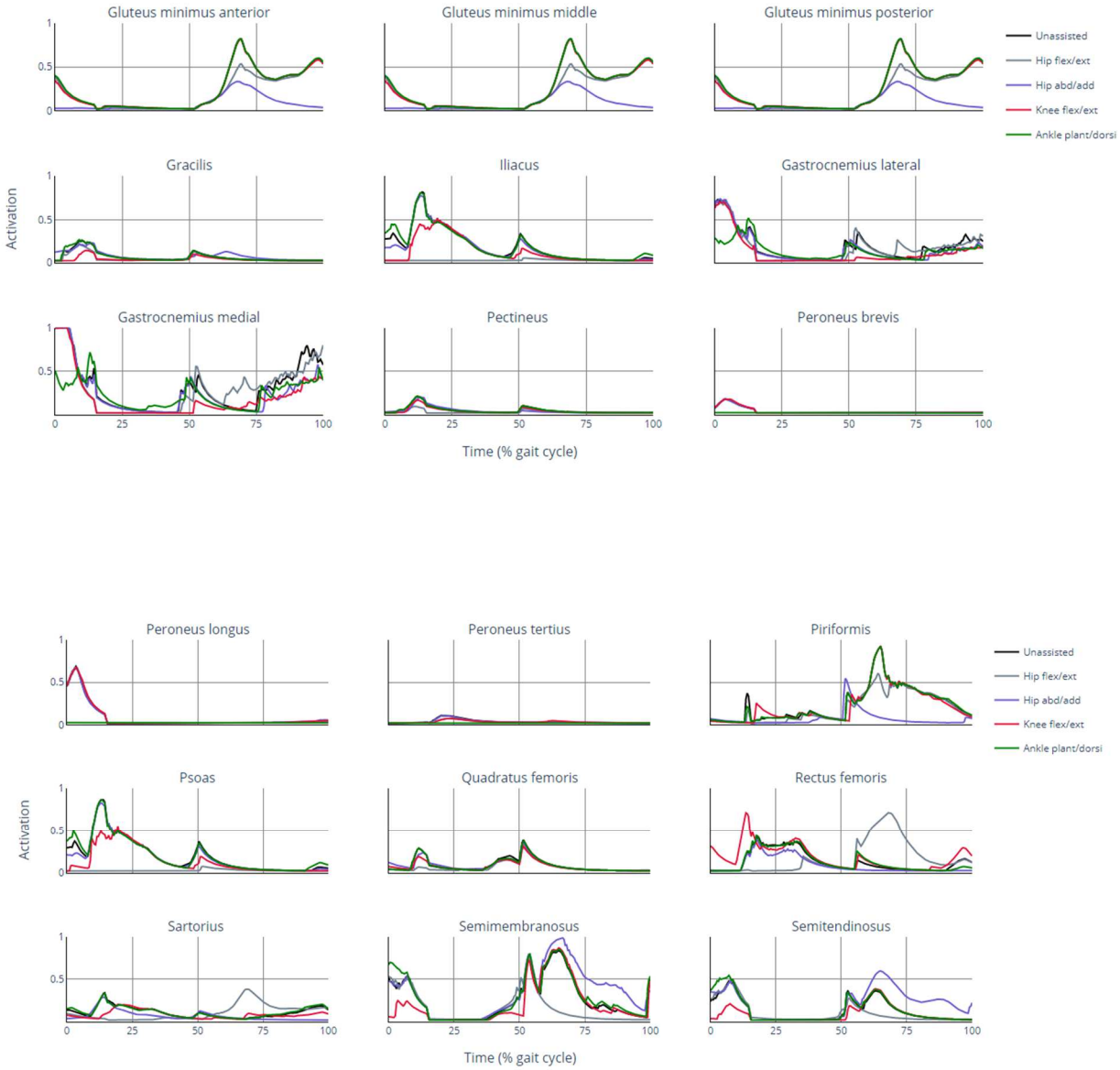

Figure B-2. Continued.

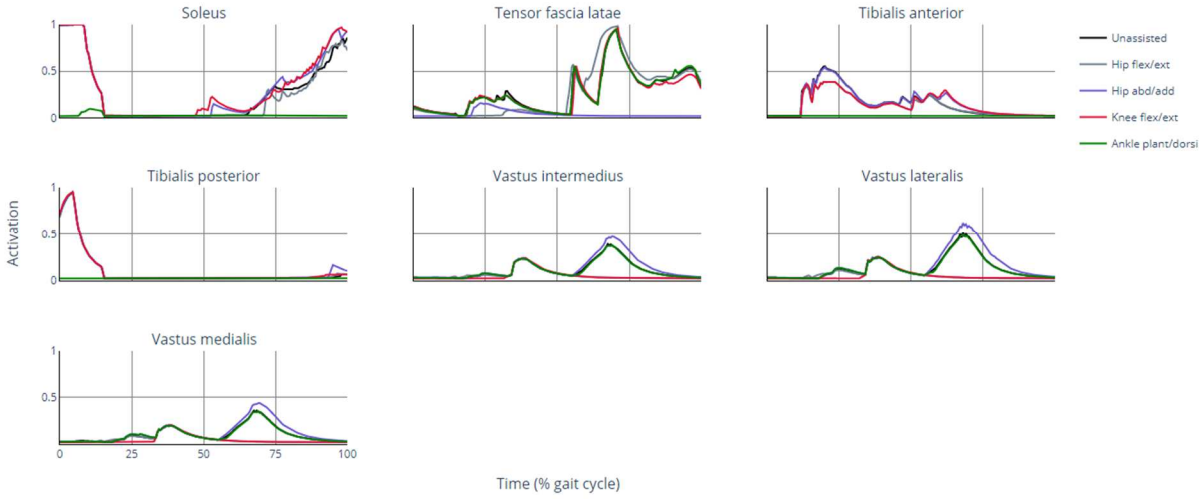

Figure B-2. Continued.